RESOURCE
https://doi.org/10.1038/s41593-020-00717-0

nature neuroscience

Mapping the epigenomic and transcriptomic interplay during memory formation and recall in the hippocampal engram ensemble

Asaf Marco[1,2]✉, Hiruy S. Meharena[1,2], Vishnu Dileep[1,2], Ravikiran M. Raju[1,3], Jose Davila-Velderrain[4], Amy Letao Zhang[2], Chinnakkaruppan Adaikkan[1,2], Jennie Z. Young[1,2], Fan Gao[1], Manolis Kellis[4,5] and Li-Huei Tsai[1,2,5]✉

The epigenome and three-dimensional (3D) genomic architecture are emerging as key factors in the dynamic regulation of different transcriptional programs required for neuronal functions. In this study, we used an activity-dependent tagging system in mice to determine the epigenetic state, 3D genome architecture and transcriptional landscape of engram cells over the lifespan of memory formation and recall. Our findings reveal that memory encoding leads to an epigenetic priming event, marked by increased accessibility of enhancers without the corresponding transcriptional changes. Memory consolidation subsequently results in spatial reorganization of large chromatin segments and promoter–enhancer interactions. Finally, with reactivation, engram neurons use a subset of de novo long-range interactions, where primed enhancers are brought in contact with their respective promoters to upregulate genes involved in local protein translation in synaptic compartments. Collectively, our work elucidates the comprehensive transcriptional and epigenomic landscape across the lifespan of memory formation and recall in the hippocampal engram ensemble.

The formation and preservation of long-term memories depends on coordinated gene expression and synthesis of synaptic proteins[1]. These molecular processes act within a specific population of neurons, referred to as engram cells[2–4]. Recent approaches using activity-dependent expression of reporters provided a framework for exploring the engram ensemble[5–8], but the molecular mechanisms that govern memory storage and retrieval remain poorly understood. Specifically, epigenetic modifications and the 3D genome architecture are emerging as key factors in the dynamic regulation of gene expression[9–17], and there is an increasing appreciation of their importance in neuronal function, development and disease[14,16,18]

In this study, we used the targeted recombination in active populations (TRAP) mouse model[5,6], in which activated neurons expressing the activity-regulated cytoskeleton-associated protein (*Arc*) gene are permanently tagged in an inducible manner. Activated neurons during memory encoding, consolidation and recall were sorted and subjected to nuclear RNA sequencing (nRNA-seq), assay for transposase-accessible chromatin using sequencing (ATAC-seq) and chromosome conformation capture (Hi-C). Our data demonstrate that memory encoding leads to a genome-wide increase in chromatin accessibility, without expected changes in gene expression. Furthermore, we demonstrate that late phase of memory consolidation was associated with re-localization of large chromatin segments (sub-compartments) from inactive to permissive environments and reorganization of the promoter–enhancer interaction landscape. Finally, reactivation of the neurons during memory recall is associated with de novo promoter–enhancer interactions, using a large subset of the enhancers that were primed during memory encoding. These promoter–enhancer interactions are associated with a robust change in the expression of genes involved in local protein synthesis and synaptic morphogenesis.

Results

Temporal and spatial identification of activated and reactivated engram cells. Tracking neuronal activity over time has been one of the major challenges when studying engram cells, as the markers for neuronal activity, known as immediate early genes (IEGs), return to baseline shortly after induction[1,2]. To overcome this limitation, we took advantage of the TRAP[5,6] model, which requires two transgenes, one that expresses CreERT2 from an activity-dependent Arc promoter and one that allows expression of the yellow fluorescent protein (eYFP) reporter, in a Cre-dependent manner. Administration of tamoxifen (TAM) to the TRAP mice results in a permanent eYFP label in the activated Arc neurons. Without TAM, CreERT2 is retained in the cytoplasm and eYFP is not expressed (Extended Data Fig. 1a). TRAP mice were subjected to the classic Pavlovian contextual fear conditioning (CFC) paradigm (Fig. 1a), a commonly employed method to study aversive memories[19]. Approximately 1.5–2 h after exposure to foot shock (FS), brains were collected to identify 1) RNA-binding protein fox-1 homolog 3 (Rbfox3), also known as NeuN$^+$ and eYFP$^+$ tagged neurons, that were activated during the initial exposure (Activated-early), which can be distinguished from 2) NeuN$^+$/eYFP$^-$ non-activated basal-state neurons (Basal) (Fig. 1a). After 5 d, in the absence of retrieval, we collected 3) NeuN$^+$eYFP$^+$ neurons that were tagged on the training day, denoting long-term memory consolidation (Activated-late). In a different cohort, mice were re-exposed to

[1]Picower Institute for Learning and Memory, Massachusetts Institute of Technology, Cambridge, MA, USA. [2]Department of Brain and Cognitive Sciences, Massachusetts Institute of Technology, Cambridge, MA, USA. [3]Division of Newborn Medicine, Boston Children's Hospital, Harvard Medical School, Boston, MA, USA. [4]Computer Science and Artificial Intelligence Laboratory, Massachusetts Institute of Technology, Cambridge, MA, USA. [5]Broad Institute of Harvard and MIT, Cambridge, MA, USA. ✉e-mail: marcoa@mit.edu; lhtsai@mit.edu

the conditioned stimulus, and subsequent endogenous Arc protein expression was assayed 1.5–2 h after re-exposure. This enabled the identification of 4) double-positive NeuN$^+$eYFP$^+$ endogenous Arc$^+$ engram neurons that were activated during training and reactivated during memory recall (Reactivated). Notably, although DNA recombination might not fully occur 1.5–2 h after the FS, we observed high co-localization (average of 84%) between endogenous Arc protein and the Arc:eYFP reporter (Extended Data Fig. 1b), which was also consistent with previous reports[20].

To confirm memory encoding and recall during CFC, freezing behavior was recorded during training and re-exposure to fear-inducing cues (Extended Data Fig. 1c). Consistent with previous publications[6,20], our data showed a significant increase in the number of eYFP$^+$ (Activated-early and Activated-late) neurons in the hippocampus compared to mice that remained naive to CFC in their home cage ($F_{2,70}$ = 240.3, P < 0.0001; Fig. 1b). Activity-dependent tagging was also negligible (~1%) in the absence of TAM induction (Fig. 1c and Extended Data Fig. 1d). With TAM treatment, we observed a wide distribution of activity-labeled populations across all hippocampal sub-regions, where early activation was predominantly observed in the dentate gyrus (DG), and late tagging was most abundant in the CA1 (Fig. 1d). To further interrogate the specificity of engram formation, we subjected TRAP mice to CFC learning in context A and then exposed them 5 d later to the same context (A–A) or to a novel neutral context B (A–B) (Fig. 1e and Extended Data Fig. 1e). We found similar numbers of Activated-late neurons in both groups (P = 0.9) and significantly fewer Reactivated neurons in the A–B group (P < 0.0001; Fig. 1f and Extended Data Fig. 1f), confirming that the reactivated cells play a key role in encoding previous experience.

Memory formation is associated with increased chromatin accessibility, predominantly on enhancers. To better understand the molecular forces that govern different transcriptional programs, we measured genome-wide changes of chromatin accessibility across different phases of memory. Hippocampal tissues were pooled, and isolated nuclei were subjected to ATAC-seq library preparation (Extended Data Fig. 2a and Supplementary Table 1). Differentially accessible regions (DARs) analysis (Diffbind, DESeq2) between all populations (Fig. 2a) revealed that most changes in chromatin state occur during the early phase of memory formation, where 7,862 regions across the genome gain accessibility (Basal versus Early; Supplementary Table 2). In contrast, we observed relatively minimal changes in chromatin state when transitioning from Activated-early to Activated-late (582 DARs) and between Activated-late and Reactivated neurons (725 DARs), with 48% overlap between them (Extended Data Fig. 2b). Remarkably, we identified a large percentage (52%) of stably gained DARs that became more accessible in Activated-early and remained accessible in both the Activated-late and Reactivated neurons (Fig. 2b,c and Supplementary Table 2). Interestingly, whereas both early changes (Basal versus Early) and stably gained DARs were enriched for intergenic regions, late chromatin changes (Early versus Late and Late versus Reactivated) were mostly enriched for promoter sites (Fig. 2d).

Functional insight was afforded by assessing how DARs are marked by different histone modifications. We first used ChromHMM to establish a chromatin state model from two independent studies that used bulk hippocampus tissue before and after FS[21,22]. Next, we performed a fold enrichment (FE) analysis (observed over expected distribution) of the DARs for these different states and revealed that early chromatin changes and stable DARs were enriched for enhancer marks (Fig. 2e, Extended Data Fig. 2c and Supplementary Table 3). These results are in line with previous publications showing that stimulating primary neuronal culture induces prolonged enhancer activity[12,23]. Next, we analyzed the overlap of individual stable loci with the H3K4me1 and H3K27ac[21]. These two histone marks delineate different populations of enhancers, which can be 'primed' (only H3K4me1), 'active' (H3K4me1 and H3K27ac) or 'latent' (no marks)[18]. Stable peaks showed a distribution across both primed and active enhancers (Extended Data Fig. 2d), where 47% of these sites were predicted to be 'latent' (no overlap between DARs and histone marks[21] obtained 1 h after FS). To confirm our model, we performed chromatin immunoprecipitation (ChIP) for H3K4me1 and H3K27ac histone markers, followed by quantitative polymerase chain reaction (qPCR). Four selected sites were chosen from our putative enhancer modeling analysis (Extended Data Fig. 2d; enhancer 1, predicted primed; enhancer 2, predicted active; enhancers 3 and 4, predicted latent). In agreement with our model, we identified two 'latent' loci (enhancers 3 and 4) in the basal state that transformed to an 'active' state during memory formation (Fig. 2f). Moreover, the putative enhancer 1 was found to be 'primed' in the basal state and became 'active' where there was significant stable increase in H3K27ac markers during the late phase and recall (Fig. 2f). Together, these data indicate that the repertoire of newly accessible enhancers was expanded in the potentiated engram neurons where 'latent' or 'primed' regions gained H3K4me1 and H3K27ac marks and thus became active enhancers.

To understand the functional role of accessible promoter and enhancer regions, we performed motif enrichment analysis (Supplementary Table 4). Our data indicates that most (70%) of motifs on accessible promoters are equally enriched and were identified across all phases of memory (Extended Data Fig. 2e). In

Fig. 1 | Temporal and spatial identification of activated and reactivated engram cells. a, Schematic representation of the experimental design. TRAP mice were initially exposed to training in which a conditioned (context) and unconditioned (FS) stimulus were paired together within a brief window of TAM exposure. Four different neuronal populations (Basal, Activated-early, Activated-late and Reactivated) were sorted by a flow cytometer and subjected to library preparation for nRNA-seq, ATAC-seq, Hi-C and pc-HiC. **b**, Representative images (DG) and whole hippocampus quantifications of eYFP$^+$ neurons after TAM treatment in home cage (naive, n = 4 mice, 6 slices per animal), 1.5 h (Activated-early, n = 4 mice, 4 slices per animal) and 5 d (Activated-late, n = 4 mice, 8 slices per animal) after exposure to FS. Scale bar, 200 μm. The dot plot indicates the mean and error bars (s.e.m.), one-way ANOVA (parametric, unpaired), $F_{2,70}$ = 240.3, P < 0.0001. Bonferroni's multiple comparisons test: home cage (HC) versus Early, ***P = 0.0007; HC versus Late, ****P < 0.0001; Early versus Late, ****P < 0.0001. **c**, Quantifications of Activated-late and Reactivated neurons in the hippocampus in two experimental groups: CFC with (CFC + TAM, n = 4 mice, 8 slices per animal) or without (CFC NO-TAM, n = 4 mice, 6 slices per animal) TAM administration. The dot plot indicates the mean and error bars (s.e.m.), two-sided unpaired Student's t-test, Activated-late: t = 25.65, df = 47; Reactivated: t = 11.00, df = 52; ****P < 0.0001. **d**, Representative images and quantifications from different regions of the hippocampus. Number of positive nuclei analyzed using IMARIS (Methods) from the DG, CA1 and CA3: n = 5 mice, Activated-early, 6 slices per animal; n = 6 mice, Activated-late, six slices per animal; Reactivated: six slices per animal. Scale bar, 100 μm. The dot plot indicates the mean and error bars (s.e.m.), one-way ANOVA (parametric, unpaired), Early: $F_{2,42}$ = 13.46; Late: $F_{2,95}$ = 556.3; Reactivated: $F_{2,89}$ = 83.53. All P < 0.0001. Bonferroni's multiple comparisons test, *P = 0.029, **P = 0.0075, ***P = 0.0009, ****P < 0.0001. **e**, Valuation of context effects on the number and distribution of hippocampal memory traces. **f**, Quantifications of Activated-late and Reactivated neurons in the A–B group (n = 6 mice, 6 slices per animal) compared to the A–A group (n = 5 mice, 6 slices per animal). The dot plot indicates the mean and error bars (s.e.m.), two-sided unpaired Student's t-test, Activated-late: t = 0.08292, df = 59, P = 0.9342; Reactivated: t = 8.385, df = 57, ****P < 0.0001. NS, not significant.

contrast, most enhancer sites showed distinct patterns of transcription factor (TF)-binding motifs across different memory phases. Interestingly, the ubiquitously expressed motifs from the Jun proto-oncogene, the Ap1 TF subunit (that is, Jun-Ap1) and the regulatory factor X (Rfx) family of TFs were significantly enriched only after the initial phase of encoding (Extended Data Fig. 2e). It was previously reported that Jun-Ap1 complex plays a central role in enhancer selection and might act as a pioneer TF to define enhancer sites during brain development and neuronal activity[12,24]. These findings are consistent with our data that showed a high percentage of latent/primed loci in the basal state (Fig. 2f and Extended Data Fig. 2c,d). Hence, it appears that neuronal activity might trigger the binding of Jun-Ap1 to latent enhancers, which then recruits chromatin modifiers that activate latent enhancers. Similarly, the enrichment of the TF yin yang 1 (Yy1) motifs only in enhancers from the early and late states suggests that promoter–enhancer organization is an active process of memory formation, as it was recently reported that Yy1 facilitates the formation of these long-range interactions[25]. Collectively, these data suggest that the initial phase of memory formation alters the chromatin accessibility landscape in activated neurons, with long-lasting stable changes occurring predominantly within enhancer regions.

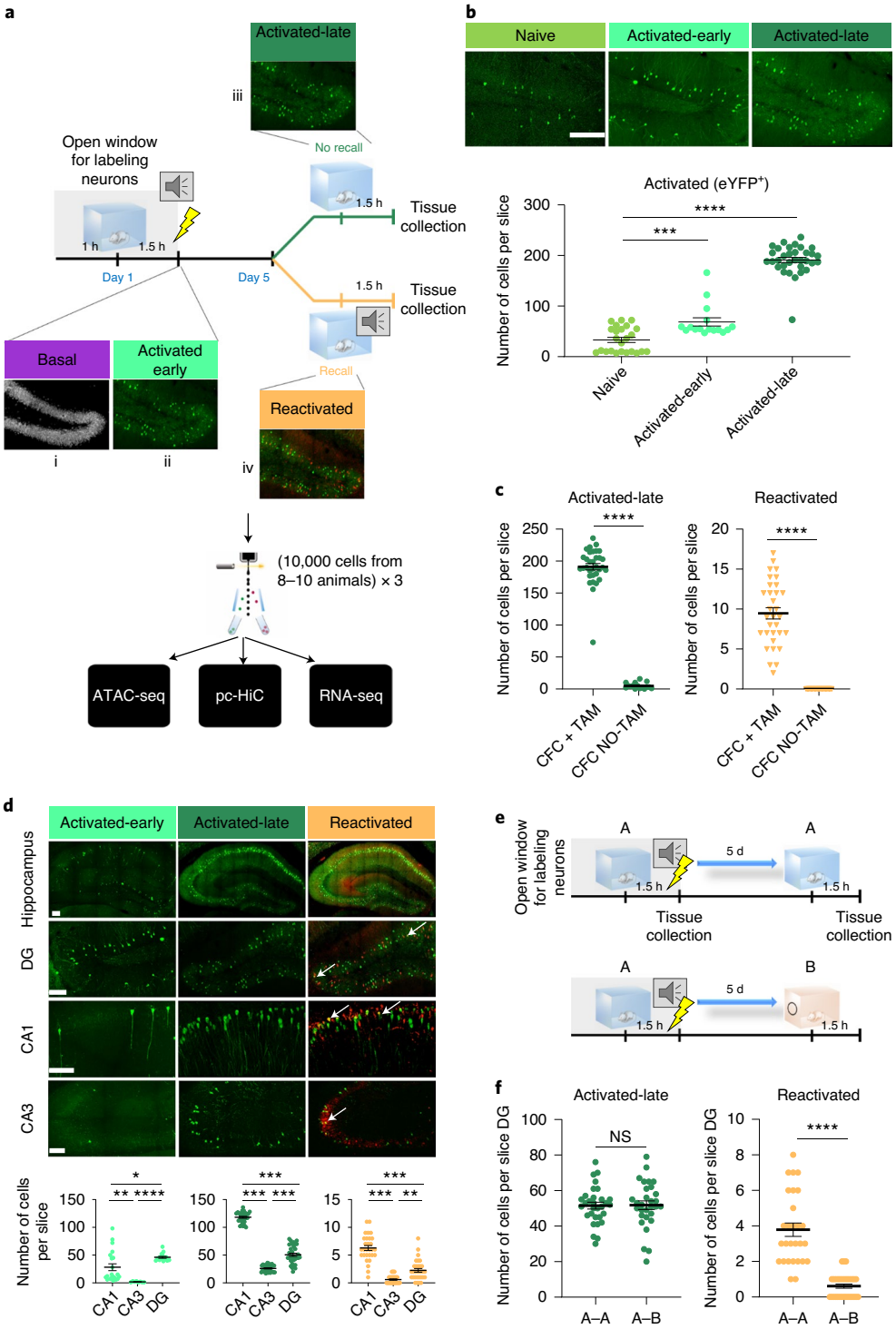

Dynamic changes in spatial nuclear architecture and chromatin accessibility during initial memory formation correspond with increased promoter–enhancer interaction frequency during memory recall. Nuclear 3D architecture is emerging as a key factor in dynamic regulation of gene expression in many neuronal functions[26–28]. Hence, we were interested in delineating the precise changes that occur in spatial chromatin organization during memory formation and consolidation. We produced Hi-C data from basal state and eYFP$^+$ tagged neurons (early and late; Supplementary Table 5). Chromatin is segregated into two spatially distinct sub-nuclear compartments, 'A' and 'B', corresponding to trasncriptionally active and inactive chromatin, respectively[15,16,26]. Early evidence suggests that neuronal activity and extrinsic signaling might induce a reorganization of 3D chromatin architecture[14,27,28]. Our compartment state analysis[15,16,26] (Fig. 3a–c) revealed re-localization of large chromatin segments from inactive (B) to permissive environment (A) (and vice versa) during the initial and late phase of memory formation (212 segments switched from A to B, 127 from B to A, average size of ~436 kbp). Interestingly, 52% of the regions in the early phase that switched from B to A maintained that state in the late phase (that is, remained in state A; Fig. 3b,c and Supplementary Table 6). Moreover, nearly all these regions overlapped with gained DARs from our ATAC-seq analysis, confirming the transition of sub-compartments from inactive to permissive environments (Fig. 3d). These data indicate that some loci undergo sub-compartment switching across different memory phases and therefore might contribute to long-term changes in neuronal properties and function after initial activation.

Although our Hi-C data suggested large-scale reorganization, it remained unclear whether this reorientation enabled the interaction of novel promoter–enhancer repertoires and the fine-tuning of different transcriptional programs (Fig. 3e). By using the promoter capture Hi-C (pc-HiC) technique, we studied the precise changes that occur in promoter–enhancer interactions during the process of memory formation and recall. For this study, we used custom-designed 'baits' targeting ~5,000 promoters[29]. In agreement with previous publications[29], we detected ~19,000 (per group) significant promoter–enhancer (67.5%) and promoter–promoter (46.2%) interactions (Extended Data Fig. 3a,b).

Because promoters in the mammalian brain could be under the control of multiple regulatory elements[14,30,31], we analyzed the overlap between all interacting enhancers and their respective promoters. We found that, during each memory phase, the same promoters interact more frequently with a distinct subset of enhancers (that is, unique: Basal, 3,243; Early, 7,602; Late, 7,028; and Reactivated, 7,244; Fig. 4a,b, Extended Data Fig. 3c and Supplementary Table 7). This result is consistent with previous publications showing that multiple enhancers surrounding several genes (c-Fos and Arc) are crucial for their activation, and their interaction frequency with their respective promoters is altered in response to various depolarizing agents in cultured neurons[31]. We also identified a smaller subset of interactions in which the promoters were interacting with the same enhancers across different memory phases (that is, common, ~31% of all interactions; Supplementary Table 7). Furthermore, Reactivated neurons presented significantly stronger interaction scores (as calculated by CHiCAGO; Fig. 4b and Extended Data Fig. 3d). Hence, although the number of unique interactions was similar across Early, Late and Reactivated states, stronger interaction scores indicate that specific promoter–enhancer interactions occur more frequently during memory recall. This notion was further validated by 3C experiments, with primers designed to measure the frequency of interaction between selected enhancers (E) and gene promoters (P) that encode for eukaryotic translation initiation factor 3 subunit D (Eif3d) or glutamate receptor, ionotropic, kainate 3 (Grik3) (Fig. 4c). Our data showed that Reactivated neurons had a significant increase in the interaction frequency between the Eif3d promoter and the selected enhancer compared to the other populations (Fig. 4c). Collectively, these data indicate that promoter–enhancer interactions occur more frequently during memory recall.

Next, we asked whether the dynamic long-range interactions identified via pc-HiC correspond to chromatin regions that become more accessible, as determined via ATAC-seq. This would confirm that the increased accessibility has a functional consequence in bringing about novel promoter–enhancer interactions. To achieve this, we compared the overlap between interacting enhancers in each cell population to DARs (observed) or a random set of accessible genomic loci (expected). Our analysis revealed a significant overlap between both gained DARs in Activated-early neurons and stably gained DARs with the interacting enhancers in all cell populations (all P values < 0.0001; Extended Data Fig. 3e). In contrast, changes in chromatin accessibility that occurred during the late phase of memory consolidation and reactivation did not significantly overlap with interacting enhancers (Extended Data Fig. 3e). Together, these results indicate that the gain of accessibility during memory encoding is a priming event, and these primed loci engage in de novo functional promoter–enhancer interactions during later phases of memory formation. This dynamic landscape is illustrated by visualizing the genomic regions around the eukaryotic translation initiation factor 5 subunit A (Eif5a) gene (Fig. 4d). This temporal molecular dissection of the engram lifespan highlights how a coordinated priming of the epigenetic state of a cell during memory encoding and consolidation facilitates long-range interactions during reactivation.

Fig. 2 | Chromatin accessibility landscape during memory formation and recall. a, DARs are shown in a volcano plot (pairwise comparisons, FDR < 0.01, FCs > 1.5), $n = 3$ biologically independent samples. **b**, Analysis of common gained accessible regions (stable), acquired 90 min after the FS (Activated-early), that remain accessible in the late state of consolidation (Activated-late) and recall (Reactivated). Overlapping stable DARs were considered only if they appeared in at least two biological replicates in a given condition. **c**, Representative IGV genome browser tracks of the Arc locus. **d**, Annotation analysis (HOMER tools) for all the DARs. Numbers on the y axis indicate the $\log_2$ ratio values of observed loci (number of DARs) over expected (total size (bp)) of the TTS, exons, introns, intergenic and promoters. P values were calculated by HOMER tools; Basal versus Activated-early (Intergenic, $^*P = 1.73 \times 10^{-103}$), Activated-early versus Activated-late (TTS, $^*P = 0.0339$; Promoter, $^*P = 1.48 \times 10^{-39}$), Activated-late versus Reactivated (Promoter, $^*P = 2.48 \times 10^{-6}$), stable (Intergenic, $^*P = 0.0358$). **e**, Histone modification emission states (left) and enrichment analysis of DARs over emissions using ChromHMM. FE scale, 0–30. The P value was determined by the z score value (as calculated in Extended Data Fig. 2c). Full analysis is reported in Supplementary Table 3. $^*P < 0.00001$, reported only for enriched values (not depleted). **f**, ChIP-qPCR. Samples were immunoprecipitated with antibodies against H3K27ac or H3K4me1 and subjected to real-time PCR with two sets of primers for identified putative enhancers. H3K27ac: $n = 4$; H3K4me1: $n = 3$. The dot plot indicates the mean and error bars (s.e.m.), one-way ANOVA (parametric, unpaired) with Dunnett's multiple comparisons test. Enhancer 1: H3K27ac: $F_{3,12} = 4.664$, $P = 0.02$ (Basal versus Activated-late, $^*P = 0.0246$; Basal versus Reactivated, $^*P = 0.0232$); H3K4me1: $F_{3,8} = 0.845$, $P = 0.506$. Enhancer 2: H3K27ac: $F_{3,12} = 5.221$, $P = 0.0155$ (Basal versus Activated-late, $^{**}P = 0.0059$); H3K4me1: $F_{3,8} = 1.719$, $P = 0.24$. Enhancer 3: H3K27ac: $F_{3,12} = 29.91$, $P < 0.0001$; H3K4me1: $F_{3,8} = 10.39$, $P = 0.0039$ (Basal versus Activated-early, $^*P = 0.0298$; Basal versus Activated-late, $^{**}P = 0.0021$; Basal versus Reactivated, $^{**}P = 0.0063$). Enhancer 4: H3K27ac: $F_{3,12} = 6.273$, $P = 0.0083$ (Basal versus Activated-late, $^{**}P = 0.007$; Basal versus Reactivated, $^*P = 0.0152$); H3K4me1: $F_{3,8} = 9.901$, $P = 0.0045$ (Basal versus Reactivated, $^{**}P = 0.0016$).

Distinct transcriptional programs of the engram ensembles during memory formation and recall. To elucidate how changes in chromatin accessibility and promoter–enhancer interactions were affecting gene expression, we performed nRNA-seq from all the neuronal subpopulations. Our differentially expressed gene (DEG) analysis revealed a low amount of changes in the early phase compared to basal state neurons (Basal versus Early, 88 DEGs; Fig. 5a and Supplementary Table 8). This was especially unexpected given the extensive degree of chromatin reorganization observed at this time point (Fig. 2a). In contrast, neurons from the late phase presented higher numbers of DEGs despite there being more similarity in chromatin accessibility at these time points (Fig. 5a). To validate our transcriptional findings, we compared our results to previously published data of activated DG granule cells 1 h after novel exposure[32], 24 h after FS[20] and after prolonged stimulation (6 h) of mouse cultured cortical neurons with KCl[33] (Extended Data Fig. 4a).

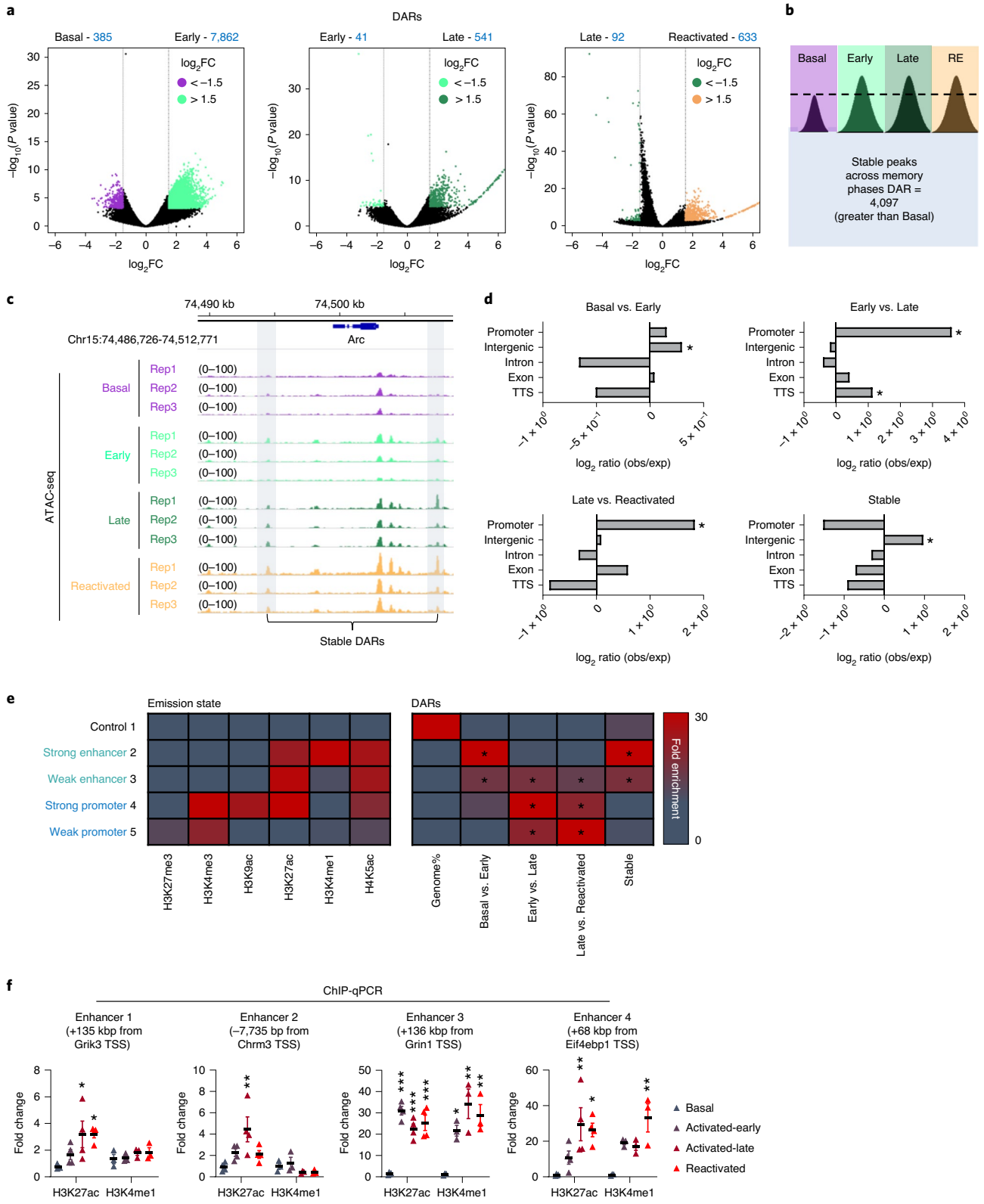

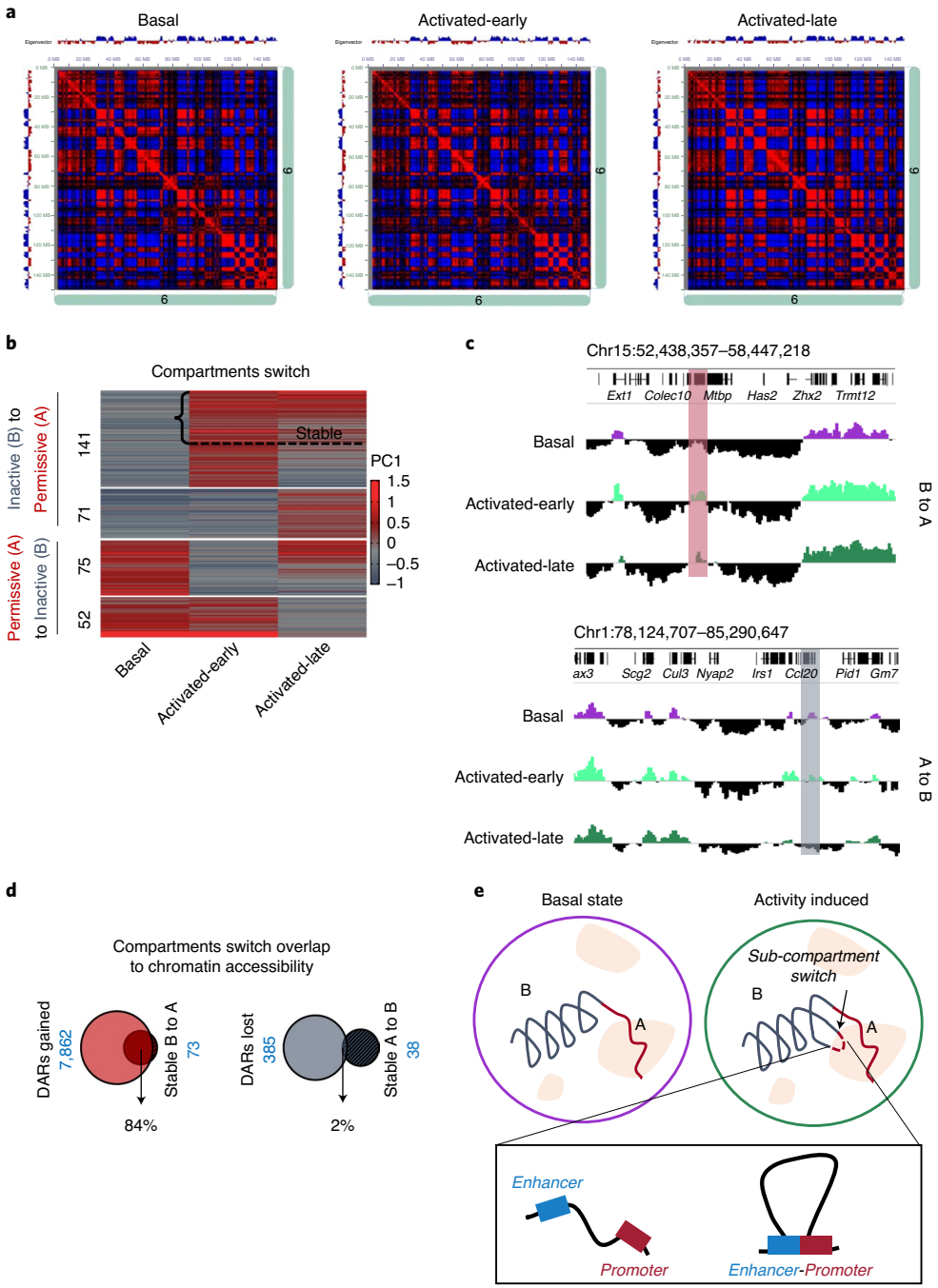

Fig. 3 | Sub-compartment switching across the different phases of memory formation and recall. a, Hi-C correlation heat map represents compartmentalization of chr6 for Basal, Activated-early and Activated-late cells. Compartments calculated by Juicer at 500-kb resolution (observed-expected normalized). **b**, Dynamic changes in compartment state. Positive values of the first component (+PC1) reflecting active chromatin and negative values (−PC1) indicative of inactive chromatin state were compared among all three populations of neurons (Basal, Activated-e arly and Activated-late). Compartment switch was considered only if a negative value was transformed to a positive value and vice versa. **c**, Representative images from the IGV browser that shows stable compartment switch from A to B (top) and B to A (bottom) across different memory phases. **d**, Overlap analysis between DARs in the early phase (Basal versus Activated-early) and stable switched compartment. Left Venn diagram shows gained DARs and stable compartment switched from B to A. Right Venn diagram shows lost DARs and stable compartment switched from A to B. **e**, Illustration of activity-induced compartment switch and specific promoter–enhancer interactions.

Interestingly, although this comparison revealed significant overlap between upregulated genes from our data set and 1 h after novel exposure[32] ($P=0.006$) or 24 h after FS[20] ($P=0.0005$), we did not observe any significant overlap with genes that were upregulated in the reactivated engram cells and the other data sets, confirming the unique transcriptional landscape of reactivated engram cells during recall.

Next, we took advantage of a previously published computational approach[34] that measures changes in mature RNA (exons) and pre-mRNA (introns) reads. As expected, exonic changes correlated with global transcriptional changes as measured by DEseq2 (both exon and intron reads) across all memory phases (Extended Data Fig. 4b). However, measurement of the exon/intron ratios indicates that altered

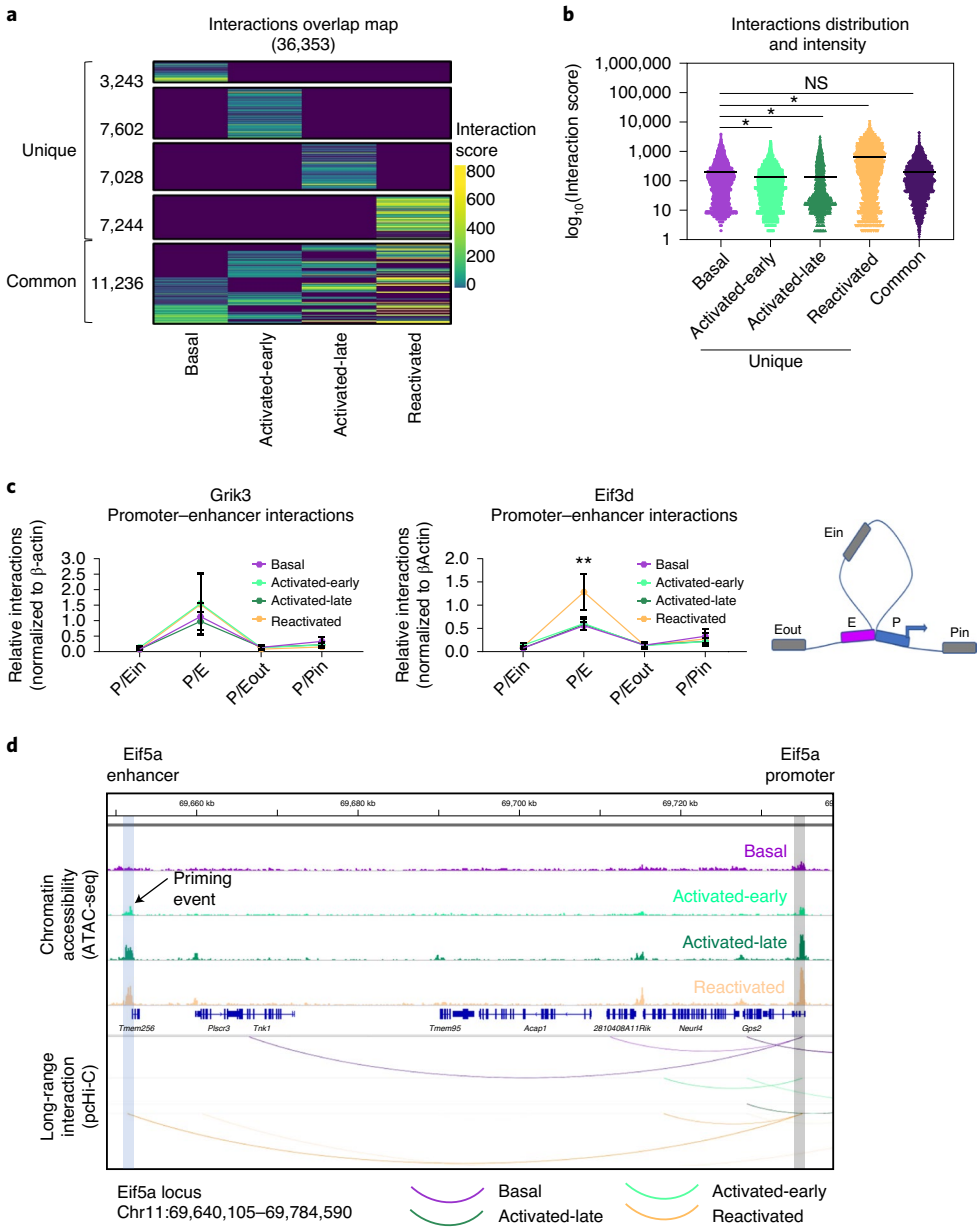

Fig. 4 | Promoters interact more frequently with a distinct subset of enhancers during each memory phase. a, Heat map represents the interaction score as defined by CHiCAGO for each population. Basal: $n=3$, Activated-early, Activated-late and Reactivated; $n=4$ biologically independent samples each. **b**, Violin plots show the distribution and the intensity ($\log_{10}$ scale) of interactions that were either unique or shared by at least three populations (common). One-way ANOVA (parametric, unpaired), $F_{4,57922} = 2{,}364$, $P < 0.0001$. Bonferroni's multiple comparisons test; NS, not significant ($P = 0.7659$), $^{*}P < 0.0001$. **c**, Frequency of promoter–enhancer interactions as measured by 3C-qPCR for selected loci. Four sets of primers encompassing interaction among promoter–enhancer (P/E) and three random loci inside the loop (P/Ein), outside the loop (P/Eout) and on the promoter (P/Pin). Reads were normalized to promoter–enhancer interaction values of the housekeeping gene β-actin. $n=3$ biologically independent samples. Data are presented as mean values with error bars indicating the s.e.m., two-way ANOVA. Eif3d; population × interaction location ($F_{9,32} = 1.917$, $P = 0.0851$), effect of interaction location only ($F_{3,32} = 22.64$, $P < 0.0001$). Grik3; population × interaction location, $F_{9,32} = 0.1716$. Bonferroni's multiple comparisons test, P/E Basal versus Reactivated, $^{**}P = 0.0019$. **d**, Representative priming events of the Eif5a locus. IGV genome browser tracks presenting chromatin accessibility dynamics (colored tracks) on promoters (gray rectangle) and enhancers (blue rectangle). WashU browser tracks presenting significant promoter–enhancer interactions via arcs (purple, Basal; light green, Activated-early; dark green, Activated-late; orange, Reactivated).

transcripts (upregulated and downregulated) during memory consolidation (Early versus Late) are predominantly driven by intronic reads, suggesting that this transcriptional profile mostly reflects immature transcripts that require additional steps of RNA processing (Extended Data Fig. 4c). In contrast, upregulated genes during recall (Late versus Reactivated) are predominantly driven from exonic transcripts, thus reflecting a more mature state of RNA (Extended Data Fig. 4c).

To reconcile the discrepancy between the observed chromatin changes and the transcriptional state in each sub-population, we performed correlation analysis of the DARs and DEGs, identified during the different time points of memory formation and recall. For this analysis, DARs on the non-coding regions (intergenic and intronic) were mapped to their respective promoters by using our pc-HiC data. Overall, we found low correlation ($P = 2.81 \times 10^{-2}$)

between differential chromatin accessibility and gene expression changes that occur in the early phase (Basal versus Early; Extended Data Fig. 4d). These results were in line with previous work[21] reporting that histone modifications have little correlation with transcriptional alterations during memory acquisition. Unexpectedly, we observed a stronger overlap and similarity between the chromatin changes that occur during memory encoding (Early) with the altered transcriptional landscape during memory consolidation (Late) and reactivated engram neurons ($P = 1.13 \times 10^{-8}$ and 2.42×10^{-7}, respectively; Extended Data Fig. 4d). To further confirm this analysis, we performed a Pearson's correlation between $\log_2$ fold change (FC) values from DARs and $\log_2$FC values of DEGs that were annotated to those regions (intergenic regions were mapped via the pc-HiC data set; Extended Data Fig. 4e and Supplementary Table 9). Our analysis revealed that early chromatin changes (Basal versus Early, DARs) were significantly correlated with downregulation of genes in the late phase (Early versus Late; Extended Data Fig. 4e, gray line, $r = -0.14$, $P < 0.0001$). Moreover, after parsing the DEGs to intronic and exonic reads, we observed that the correlation was largely driven by intronic reads (Introns $r = -0.21$, $P < 0.0001$; Exons $r = -0.09$, $P = 0.02$). In contrast, early chromatin changes (Basal versus Early, DARs) showed positive correlation with DEGs from the reactivated cells, which was predominantly driven by exonic reads (Introns $r = -0.007$, $P = 0.73$; Exons $r = 0.11$, $P = 0.04$). These data provide further evidence for a priming event and transcriptional lag, in which chromatin changes that occur during the early phase enable transcriptional changes observed at a later time point, primarily in reactivated engram cells.

Memory encoding, consolidation and recall is a dynamic process requiring several waves of delayed gene transcription[12,32,33]. Hence, to identify different transcriptional programs across all memory phases, we assessed the expression of each individual gene from non-activated neurons (Basal) through early (Activated-early), late (Activated-late) and neurons that were reactivated during recall (Reactivated). All DEGs ($n = 1{,}095$) that met the cutoff criteria ($P < 0.01$, $\log_2$FC > 1) were unbiasedly clustered (k-means) (Fig. 5b,c). Four major clusters were identified: 1) 260 genes that were downregulated in the late phase (Dw-late cluster); 2) 207 genes that were upregulated in the late phase (Up-late cluster); 3) 186 genes that were upregulated in the early phase and were sustained throughout all memory phases (Stable cluster); and 4) 438 genes that were uniquely upregulated in the reactivated neurons during memory recall (Reactivation cluster). Similarly to our pairwise comparison, transcriptional changes in the Activated-late neurons correlated higher with intronic reads, and the transcriptional landscape of reactivated neurons seems to be more mature and presented higher correlation with exonic reads (Extended Data Fig. 5a,b).

We next performed a Gene Ontology (GO) analysis for each cluster (Fig. 5d) to identify enriched pathways within different memory phases. The transcriptional signature of the Dw-late cluster was enriched for genes involved in regulating 'Inhibitory synapse function', which have been shown to play a role in neuronal excitability[35,36] (Fig. 5e). In the Up-late cluster, we observed genes sets involved in positive or negative regulation of transcription, such as the v-maf musculoaponeurotic fibrosarcoma oncogene family, protein B (*Mafb*), snail family zinc finger 2 (*Snai2*) and RE1-silencing transcription factor (*Rest*) (Fig. 5e). Interestingly, we found that 15% (32/207) of the gene's promoter in the Dw-late cluster harbor either Snai2 ($P = 1 \times 10^{-9}$) or Rest ($P = 1 \times 10^{-3}$) binding sites. This dynamic of transcriptional regulators points to a possible interplay between the Dw-late and Up-late clusters. Notably, we found that functionally distinct neuronal ensembles exist within a single memory engram, in which FBJ osteosarcoma oncogene (Fos)- and neuronal PAS domain protein 4 (Npas4)-dependent ensembles undergo distinct synaptic modifications after CFC and drive memory-guided behaviors in opposite directions[37]. We showed that excitatory synaptic inputs promote memory generalization and inhibitory ones promote memory discrimination. Although these distinct ensembles could not be differentiated in the current study, these observations might explain the bi-directional expression of positive or negative transcriptional regulators, as well as upregulated and downregulated genes involved in neuronal excitability.

The Stable cluster was mostly enriched for transcripts involved in cytoskeletal, axon remodeling and hippocampal-dependent memory[38], including the light and heavy polypeptide neurofilaments (*Nefl* and *Nefh*) and myosin, heavy polypeptide 10, non-muscle (*Myh10*) (Fig. 5d,e). To visualize and track cytoskeletal-related changes on dendrites and spines, loxp-eYFP reporter (TAM dependent) was delivered by adeno-associated virus (AAV) into the DG of Arc-CreERT2 mice (Extended Data Fig. 6a). Our data revealed that Activated-late and Reactivated neurons harbor significantly higher numbers of mushroom and thin spines ($P < 0.0001$; Extended Data Fig. 6b), with no significant changes in dendritic shaft diameter ($P = 0.6$) compared to the Activated-early neurons.

The unique transcriptional signature of reactivated engram neurons (Reactivation cluster) was mostly characterized by

Fig. 5 | Transcriptional signature of reactivated engram neurons. a, Pairwise analysis of DEGs from the hippocampus of TRAP mice that were exposed to CFC are shown in a volcano plot (FDR < 0.01, $\log_2$FC > 2), $n = 3$ biologically independent samples. **b**, Heat map and (**c**) line graphs show the average transcriptional changes ($\log_2$ scale) compared to the expression at the non-activated neurons (basal). Gene sets were clustered by k-means to (1) Dw-late, (2) Up-Late, (3) Stable and (4) Reactivation clusters. Mean of $n = 3$ biologically independent samples; P values were calculated using one-way ANOVA (parametric, unpaired), followed by Bonferroni's multiple comparisons test. Dw-late, $F_{3,1032} = 42.19$; Up-Late, $F_{3,280} = 752.5$; Stable, $F_{3,764} = 92.28$; Reactivation, $F_{3,1744} = 597.4$. All $P < 0.0001$, multiple comparisons test; NS, not significant, $^{***}P < 0.0001$. **d**, GO analysis (ToppFun) for DEGs that were identified in each cluster. **e**, Representative DEGs from each cluster. $\log_2$FC from the basal state is presented in three biological replicates. The line represents the calculated average. $n = 3$ biologically independent samples, one-way ANOVA (parametric, unpaired) with Dunnett's multiple comparisons test; NS, not significant. *Gad1*: $F_{3,8} = 4.387$, $P = 0.04$; $^{*}P = 0.0268$. *Gabrb3*: $F_{3,8} = 6.184$, $P = 0.0177$; $^{*}P = 0.0441$. *Rest*: $F_{3,8} = 23.23$, $P = 0.0003$; $^{***}P = 0.0268$. *Map4k4*: $F_{3,8} = 6.244$, $P = 0.0172$; $^{*}P = 0.0151$. *Nefl*: $F_{3,8} = 12.06$, $P = 0.0024$; $^{**}P = 0.0059$, $^{**}P = 0.0014$. *Nefh*: $F_{3,8} = 21.50$, $P = 0.0003$; $^{*}P = 0.016$, $^{***}P = 0.0008$, $^{***}P = 0.0002$. *Eif5a*: $F_{3,8} = 8.482$, $P = 0.0072$; $^{**}P = 0.004$. *Eif4h*: $F_{3,8} = 26.58$, $P = 0.0002$; $^{***}P = 0.0001$. **f**, Representative images and quantification of Eif4e protein levels from Activated-early, Activated-late and Reactivated. For quantification, two separate surfaces were built on IMARIS: cell soma and dendritic shaft. The number of Eif4e puncta was measured only in those surfaces boundaries. Data for dendritic shaft are presented as a ratio between the number and the length (μm). Scale bar, 10 μm. $n = 4$ mice, 5 sections per animal; box plot indicates the mean, interquartile range and the minimum and maximum, one-way ANOVA (parametric, unpaired). Shaft: $F_{2,28} = 5.113$, $P = 0.0128$. Soma: $F_{2,43} = 3.026$, $P = 0.0589$. Bonferroni's multiple comparisons test; Shaft: Activated-early versus Reactivated, $^{*}P = 0.0324$; Activated-late versus Reactivated, $^{*}P = 0.0324$. **g**, Representative images (left) and quantification (right) of the Gria1 protein levels during different phases of memory. Three populations of neurons (Activated-early, Activated-late and Reactivated) were analyzed, based on the immunoreactivity of eYFP and endogenous Arc. For quantification, IMARIS surfaces were built on the dendritic shaft, and the number of Gria1 puncta was measured only in the surfaces boundaries (<1-μm threshold). Data are presented as a ratio between the number of puncta and the shaft length. Scale bar, 10 μm. $n = 4$ mice/5 sections per animal; box plot indicates the mean, interquartile range and the minimum and maximum, one-way ANOVA, $F_{2,16} = 15.22$, $P = 0.0002$. Bonferroni's multiple comparisons test, $^{**}P = 0.002$, $^{***}P = 0.0005$.

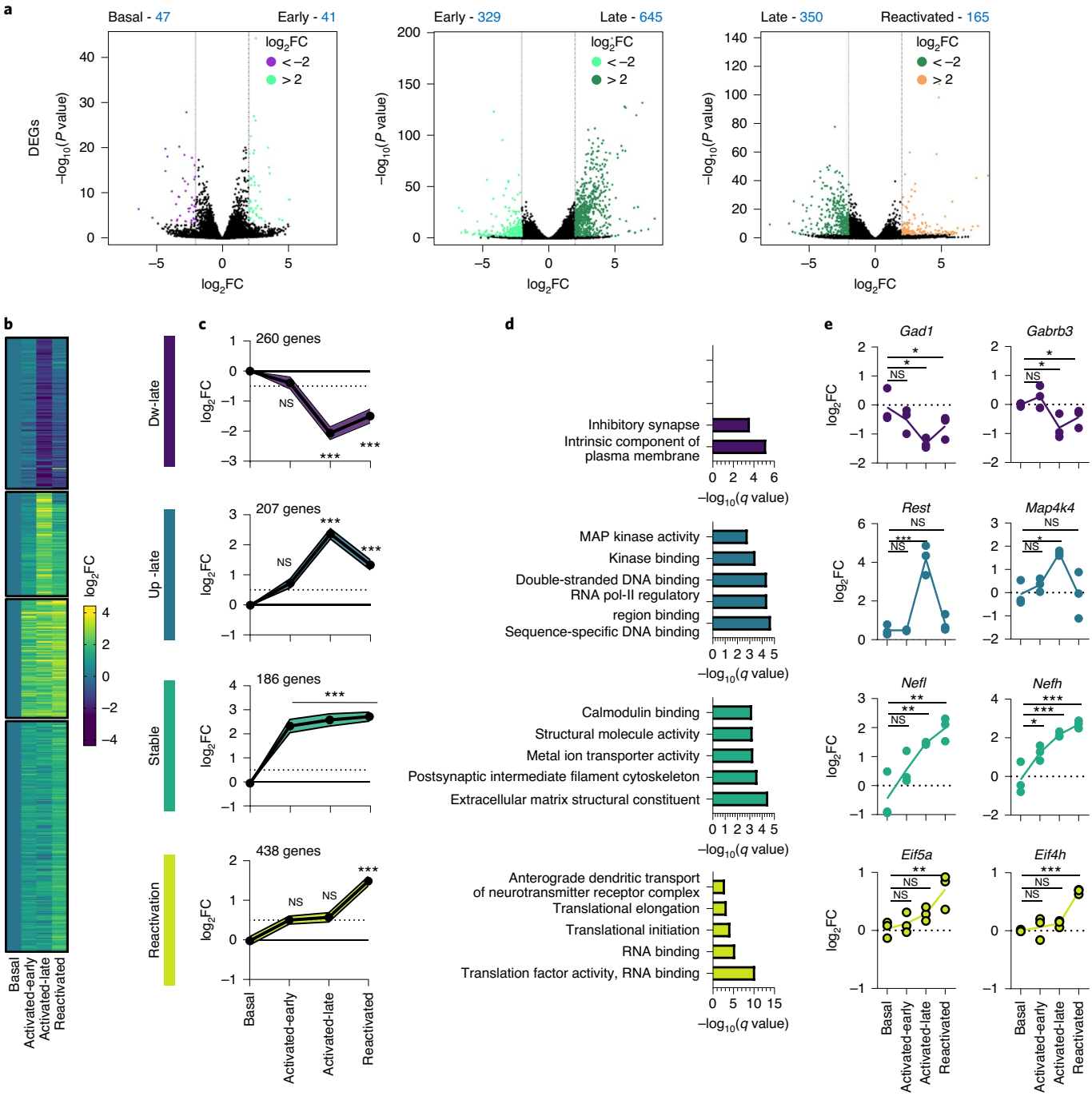
a
Basal - 47
Early - 41
Early - 329
Late - 645
Late - 350
Reactivated - 165
log2FC
< −2
> 2
DEGs
−log10(P value)
log2FC
b
log2FC
Basal
Activated-early
Activated-late
Reactivated
c
Dw-late
Up -late
Stable
Reactivation
260 genes
207 genes
186 genes
438 genes
NS
***
log2FC
Basal
Activated-early
Activated-late
Reactivated
d
Inhibitory synapse
Intrinsic component of plasma membrane
MAP kinase activity
Kinase binding
Double-stranded DNA binding
RNA pol-II regulatory region binding
Sequence-specific DNA binding
Calmodulin binding
Structural molecule activity
Metal ion transporter activity
Postsynaptic intermediate filament cytoskeleton
Extracellular matrix structural constituent
Anterograde dendritic transport of neurotransmitter receptor complex
Translational elongation
Translational initiation
RNA binding
Translation factor activity, RNA binding
−log10(q value)
e
Gad1
Gabrb3
Rest
Map4k4
Nefl
Nefh
Eif5a
Eif4h
log2FC
NS
*
**
***
Basal
Activated-early
Activated-late
Reactivated
f
Axon
Soma
Surface-GFP
GFP, Ars
Eif4E
Eif4e protein level
Activated-early
Activated-late
Reactivated
Shaft
Soma
Number puncta per length (μm)
Number puncta
g
Gria1 (protein)
GFP
Gria1
Surface-GFP
Spots-Gria1
Shaft
Number puncta per length (μm)

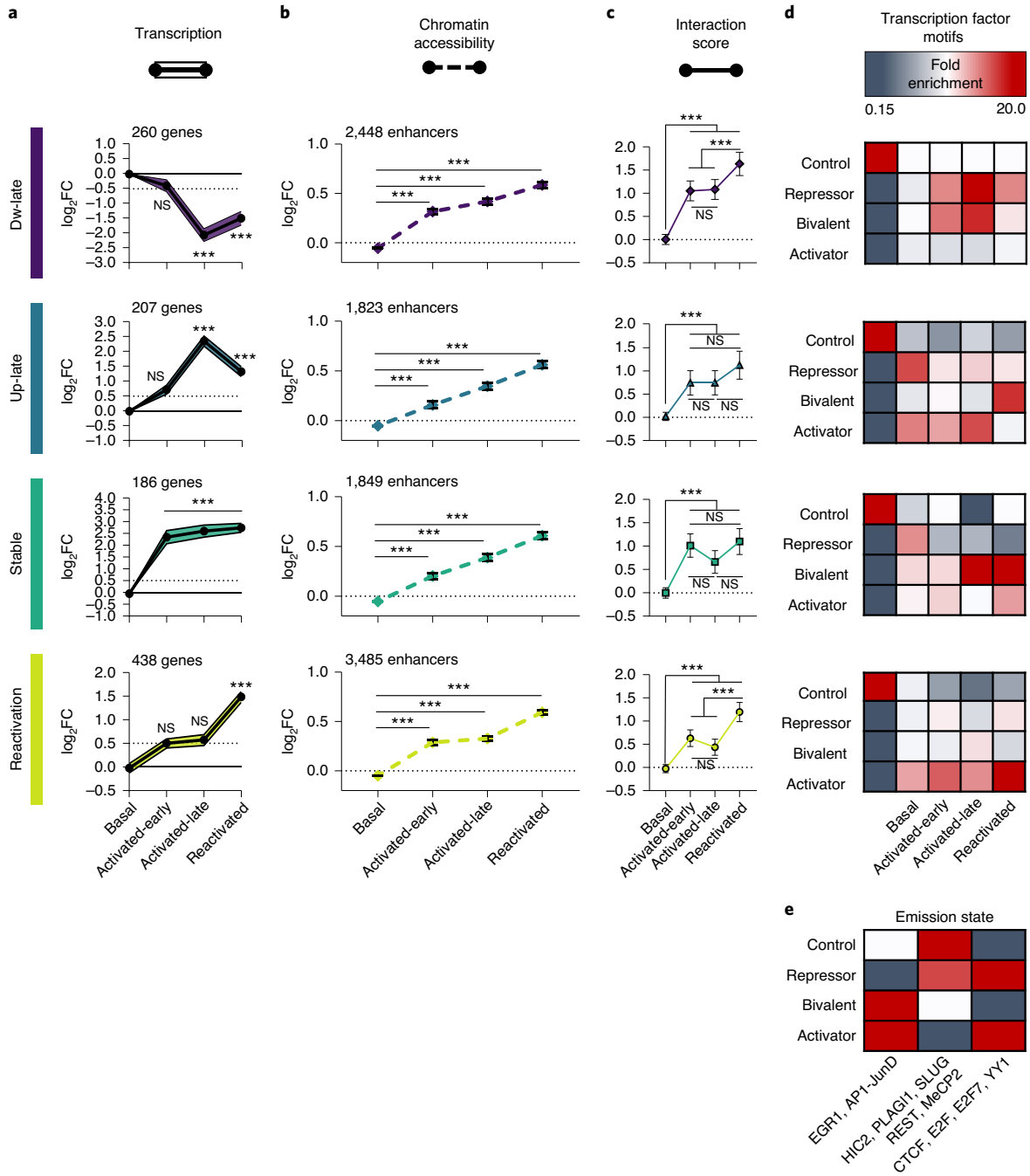

Fig. 6 | Sequential reprogramming of chromatin accessibility, promoter–enhancer interactions and gene expression over the course of engram formation. Line graphs for each *k*-means cluster shows the average (log_2 scale) of (**a**) transcriptional changes (*P* values as reported in Fig. 5c, mean of $n=3$ biologically independent samples), (**b**) chromatin accessibility (normalized RPKM values, mean of $n=3$ biologically independent samples) and (**c**) promoter–enhancer interaction scores (as calculated by CHiCAGO, mean of Basal: $n=3$, Activated-early, Activated-late and Reactivated: $n=4$ biologically independent samples each). Repeated-measures one-way ANOVA (between groups). Chromatin accessibility: Dw-late, $F_{2.359,5773} = 917.8$; Up-Late, $F_{2.519,4590} = 638.7$; Stable, $F_{2.437,4504} = 717.9$; Reactivation, $F_{2.434,8481} = 1425$. All $P < 0.0001$. Interaction scores: Dw-late, $F_{2.833,7054} = 46.86$; Up-late, $F_{2.94,5442} = 14.87$; Stable, $F_{2.91,5702} = 21.5$; Reactivation, $F_{2.86,11188} = 44.94$. All $P < 0.0001$. Bonferroni's multiple comparisons test, $^{***}P < 0.0001$. **d**, **e**, Characterization of motif enrichment on interacting enhancers in each cluster. ChromHMM was used to build the emission states using the HOMER motif database (Egr1, Ap1, Slug, Plagl1, Hic2, Rest, CTCF, Yy1 and Mecp2) and previously published ChIP-seq data (Ap1-Junb[12], CTCF[47] and Mecp2 (ref. [48])). Four states were identified as (1) control, random genome sampling; (2) strong repressors; (3) bivalent; and (4) strong activator. FE, 0.15–20.

categories of 'RNA transport/binding' and 'protein translational mechanisms' (Fig. 5d). This transcriptional program includes elevated expression of kinesin family members 5a and 5c (*Kif5a* and *Kif5c*), eukaryotic translation initiation (*Eif*) factor 3 subunit A and D (*3a* and *3d*), factor 4 subunit H (*Eif4h*), factor 5 subunit A (*Eif5a*) and ribosomal protein (*Rpl27a*, *Rpl35*, *Rpl36*, *Rps19*, *Rps24* and *Rpsa*) (Fig. 5d,e), which were previously reported to play a crucial role in the transport of mRNA to the synaptic compartment and

autonomous control of local translation[39]. To further validate these findings at the translational level, we measured protein expression and localization of three members of the Eif family by immunohistochemistry (IHC). Several Eif members were previously reported to be specifically involved in the translation in synaptic compartments[39]; hence, we separately analyzed protein expression on the soma and the dendrite shafts of activated neurons (Fig. 5f). Reactivated neurons had higher expression of Eif3e proteins in the soma compared to the Activated-early and Activated-late neurons (Extended Data Fig. 6c). In contrast, Eif4e was significantly more abundant in the shafts of the Reactivated neurons compared to Activated-early and Activated-late neurons (P values < 0.05; Fig. 5f), providing further evidence for increased protein synthesis in those neurons.

Increased translation machinery facilitates alterations in spine shape, size and number, resulting in enhanced synaptic plasticity[39–41]. Furthermore, spines with larger head diameters are more likely to contain ribosomes for local protein synthesis and larger post-synaptic densities, which anchor more AMPA glutamate receptors and make these synapses functionally stronger[41,42]. Consistent with those reports, Reactivated neurons presented a higher number of enlarged head diameters (51% from all mushroom spines) compared to the Activated-late (18%) group (Extended Data Fig. 6d). Moreover, we found a significant increase in both glutamate receptor 1, ionotropic, AMPA1 (*Gria1*) mRNA (Extended Data Fig. 6e) and Gria1 protein levels only in dendritic shafts of the Reactivated neurons compared to the Activated-early and Activated-late neurons (Fig. 5g). Collectively, these data support the hypothesis that distinct temporally separated transcriptional programs are being synchronized to maintain neuronal excitability, structural changes, protein translation and synaptic plasticity across the lifespan of the engram ensemble.

Regulatory elements with opposing transcriptional effects interact with promoters as memory progresses from encoding to recall. We next asked how long-range promoter–enhancer interaction and chromatin state could lead to the coordinated gene expression changes observed in each of the transcriptional clusters. To achieve that, we measured chromatin accessibility over enhancers that interact with promoters from each transcriptional cluster (Fig. 6a–c). In addition, the interaction score of those enhancers was plotted together against chromatin accessibility and their respective gene expression (Supplementary Table 10).

Overall, all clusters showed significant incremental increase in chromatin accessibility on enhancers. Notably, we found that chromatin accessibility occurred before 3D chromatin rearrangement and gene expression alteration, providing further support of a transcriptional lag (Fig. 6a–c and Extended Data Fig. 7a,b). Specifically, in the Reactivation cluster, our analysis revealed a bi-phasic process, in which the early phase of memory formation leads to a priming event, where enhancers become more accessible but fail to show expected changes in gene expression. Reactivation of the engram cells was associated with reorganization of promoter–enhancer interactions, where primed enhancers were brought in contact with their respective promoters in a higher frequency, and a transcriptional surge was observed (Fig. 6a–c).

It was previously suggested that promoter–enhancer interactions are highly dynamic, and interactions with distinct combinatorial enhancers lead to a directional change in gene expression, dependent on whether the enhancer harbors a repressor or activator motif[14,18]. To further probe this, we used ChromHMM to unbiasedly segregate the genome into different states defined by motif locations that bind transcriptional activators[1] (early growth response 1 (Egr1) and Ap1), transcriptional repressors[43,44] (pleiomorphic adenoma gene-like 1 (Plagl1), hypermethylated in cancer 2 (Hic2), methyl CpG-binding protein 2 (Mecp2), Snai2 and Rest) or TFs that bi-directionally affect transcription and are involved in the 3D genome architecture[25,44,45] (CCCTC-binding factor (CTCF), E2F transcription factor 1 (E2f) and Yy1). This identified three different combinatorial states of TF-binding sites: strong repressor, bivalent and strong activator (Fig. 6d,e). Interestingly, the cluster with reduction in gene expression (Dw-late) showed a progressively increasing correlation from encoding to retrieval with enhancers that harbor transcriptional repressors and bivalent motifs (Fig. 6d, upper heat map, and Extended Data Fig. 7c,d). These data indicate that, despite the observed chromatin accessibility, genes are downregulated due to repression that is emerging from these regulatory elements.

In contrast, in the Reactivation cluster, we observed an increment enrichment for enhancers that harbor transcriptional activators together with motifs that anchor loop structures (Extended Data Fig. 7c,d). Hence, it appears that, upon neuronal activity, several promoters can use a wide range of different enhancers to establish novel promoter–enhancer interactions that can differentially coordinate gene expression. In this model, the promoters of downregulated genes interact with enhancers that harbor transcriptional repressors, whereas upregulated genes are the result of promoter–enhancer interactions that bring transcriptional activators in close contact with respective promoters. Collectively, our data reveal a sequential reprogramming of chromatin accessibility, 3D genome architecture and promoter–enhancer interactions over the course of engram formation (Extended Data Fig. 8).

Discussion

The molecular underpinnings of engram formation have been an area of great interest. In this study, we took advantage of the TRAP mouse model to elucidate the dynamics of chromatin accessibility, 3D genomic architecture and gene expression across the lifespan of an engram cell. First, we directly show that memory encoding has a vast and long-lasting effect on chromatin accessibility. Once this chromatin state is established, subsequent events, such as memory consolidation and recall, appear to have a minor effect on the chromatin landscape. It is possible that the chosen time point for recall might not fully capture the chromatin events of reactivated cells, and subsequent chromatin changes might be associated with memory reconsolidation or extinction[8]. Notably, in line with previous publications[12,13,23], our data suggest that memory formation is largely an enhancer-driven phenomenon.

Second, our study provides the first comprehensive landscape of 3D genome architecture during different phases of memory formation, as we showed re-localization of large chromatin segments and specific promoter–enhancer interactions dynamic within these compartments that enable fine-tuning of different transcriptional programs. Moreover, we show that promoters of downregulated genes interact more frequently with enhancers that harbor transcriptional repressors and vice versa.

Finally, our work provides the first evidence for a functional priming event that is characterized by an initial increase in enhancer accessibility during encoding, without expected transcriptional changes. Our analysis revealed that, with reactivation, engram neurons use a subset of de novo promoter–enhancer interactions, where primed enhancers are brought in contact with their respective promoters to upregulate genes involved in mRNA transport and local protein translation in synaptic compartments. These changes corresponded to expected morphological and functional changes. Collectively, it appears that engram cells are marked at the epigenetic level, and the interplay among chromatin accessibility, 3D genome architecture and promoter–enhancer interactions describes a well-coordinated system that leads to a delayed transcriptional surge during engram reactivation.

As with any work, this study had several limitations. The use of the TAM-dependent TRAP mice allows for temporal resolution but opens a labeling window of about 12 h that could result in

nonspecific tagging of neurons that are not part of the CFC experience. Moreover, as previously suggested[37], the Arc-tagged neurons might be heterogeneous and include different ensembles that regulate both memory discrimination and generalization. In addition, any time point before 1.5–2 h (early) will not be sufficient to capture transcriptional and translational events caused by DNA recombination—that is, the expression of Cre recombinase and the final expression of the eYFP gene[5]. Hence, we think that many early transient clusters of DEGs were missed, as it was showed previously that many IEGs return to baseline levels after 2 h (except Arc[46]). Lastly, although our study focused on the hippocampus, structural and synaptic plasticity have been linked to long-term storage of information in other brain regions, such as prefrontal cortex and amygdala[2]. Future studies should determine if these epigenetic alterations might represent a global critical process involved in the long-term formation and retention of memories or if it is unique to the hippocampal circuits.

Online content

Any methods, additional references, Nature Research reporting summaries, source data, statements of data availability and associated accession codes are available at https://doi.org/10.1038/s41593-020-00717-0.

Reporting Summary. Further information on research design is available in the Nature Research Reporting Summary linked to this article.

Received: 24 January 2020; Accepted: 1 September 2020;
Published online: 5 October 2020

References

1. Alberini, C. M. Transcription factors in long-term memory and synaptic plasticity. *Physiol. Rev.* **89**, 1–46 (2014).
2. Josselyn, S. A., Köhler, S. & Frankland, P. W. Finding the engram. *Nat. Rev. Neurosci.* **16**, 521–534 (2015).
3. Albo, Z. & Gräff, J. Engram excitement. *Neuron* **101**, 198–200 (2019).
4. Poo, M-.M. et al. What is memory? The present state of the engram. *BMC Biol.* **14**, 40 (2016).
5. Guenthner, C. J., Miyamichi, K., Yang, H. H., Heller, H. C. & Luo, L. Permanent genetic access to transiently active neurons via TRAP: targeted recombination in active populations. *Neuron* **78**, 773–784 (2013).
6. Denny, C. A. et al. Hippocampal memory traces are differentially modulated by experience, time, and adult neurogenesis. *Neuron* **83**, 189–201 (2014).
7. Ramirez, S. et al. Creating a false memory in the hippocampus. *Science* **341**, 819–824 (2013).
8. Khalaf, O. et al. Reactivation of recall-induced neurons contributes to remote fear memory attenuation. *Science* **1242**, 1239–1242 (2018).
9. Levenson, J. M. & Sweatt, J. D. Epigenetic mechanisms in memory formation. *Nat. Rev. Neurosci.* **6**, 108–118 (2005).
10. Gräff, J. et al. Epigenetic priming of memory updating during reconsolidation to attenuate remote fear memories. *Cell* **156**, 261–276 (2014).
11. Nguyen, T. A. et al. High-throughput functional comparison of promoter and enhancer activities. *Genome Res.* **26**, 1023–1033 (2016).
12. Malik, A. N. et al. Genome-wide identification and characterization of functional neuronal activity-dependent enhancers. *Nat. Neurosci.* **17**, 1330–1339 (2015).
13. Su, Y. et al. Neuronal activity modifies the chromatin accessibility landscape in the adult brain. *Nat. Neurosci.* **20**, 476–483 (2017).
14. Rajarajan, P., Gil, S. E., Brennand, K. J. & Akbarian, S. Spatial genome organization and cognition. *Nat. Rev. Neurosci.* **17**, 681–691 (2016).
15. Lieberman-Aiden, E. et al. Comprehensive mapping of long-range interactions reveals folding principles of the human genome. *Science* **326**, 289–293 (2009).
16. Dekker, J. et al. The 4D nucleome project. *Nature* **549**, 219–226 (2017).
17. Yu, M. & Ren, B. The three-dimensional organization of mammalian genomes. *Annu. Rev. Cell Dev. Biol.* **33**, 265–289 (2017).
18. Shlyueva, D., Stampfel, G. & Stark, A. Transcriptional enhancers: from properties to genome-wide predictions. *Nat. Rev. Genet.* **15**, 272–286 (2014).
19. Nader, K., Schafe, G. E. & Le Doux, J. E. Fear memories require protein synthesis in the amygdala for reconsolidation after retrieval. *Nature* **406**, 722–726 (2000).
20. Rao-Ruiz, P. et al. Engram-specific transcriptome profiling of contextual memory consolidation. *Nat. Commun.* **10**, 2232 (2019).
21. Halder, R. et al. DNA methylation changes in plasticity genes accompany the formation and maintenance of memory. *Nat. Neurosci.* **19**, 102–110 (2015).
22. Park, C. S., Rehrauer, H. & Mansuy, I. M. Genome-wide analysis of H4K5 acetylation associated with fear memory in mice. *BMC Genomics* **14**, 539 (2013).
23. Kim, T. et al. Widespread transcription at neuronal activity-regulated enhancers. *Nature* **465**, 182–187 (2010).
24. Vierbuchen, T. et al. AP-1 transcription factors and the BAF complex mediate signal-dependent enhancer selection. *Mol. Cell* **68**, 1134–1146 (2017).
25. Weintraub, A. S. et al. YY1 is a structural regulator of enhancer–promoter loops. *Cell* **171**, 1573–1588 (2017).
26. Bonev, B. et al. Multiscale 3D genome rewiring during mouse neural development. *Cell* **171**, 557–572 (2017).
27. Fernandez-Albert, J. et al. Immediate and deferred epigenomic signatures of in vivo neuronal activation in mouse hippocampus. *Nat. Neurosci.* **22**, 1718–1730 (2019).
28. Yamada, T. et al. Sensory experience remodels genome architecture in neural circuit to drive motor learning. *Nature* **569**, 708–713 (2019).
29. Schoenfelder, S. et al. The pluripotent regulatory circuitry connecting promoters to their long-range interacting elements. *Genome Res.* **25**, 582–597 (2015).
30. Sanyal, A., Lajoie, B. R., Jain, G. & Dekker, J. The long-range interaction landscape of gene promoters. *Nature* **489**, 109–113 (2012).
31. Joo, J. Y., Schaukowitch, K., Farbiak, L., Kilaru, G. & Kim, T. K. Stimulus-specific combinatorial functionality of neuronal c-fos enhancers. *Nat. Neurosci.* **19**, 75–83 (2015).
32. Jaeger, B. N. et al. A novel environment-evoked transcriptional signature predicts reactivity in single dentate granule neurons. *Nat. Commun.* **9**, 3084 (2018).
33. Tyssowski, K. M. et al. Different neuronal activity patterns induce different gene expression programs. *Neuron* **98**, 530–546 (2018).
34. Gaidatzis, D., Burger, L., Florescu, M. & Stadler, M. B. Analysis of intronic and exonic reads in RNA-seq data characterizes transcriptional and post-transcriptional regulation. *Nat. Biotechnol.* **33**, 722–729 (2015).
35. Chandra, D. et al. GABAA receptor 4 subunits mediate extrasynaptic inhibition in thalamus and dentate gyrus and the action of gaboxadol. *Proc. Natl Acad. Sci. USA* **103**, 15230–15235 (2006).
36. Pignatelli, M. et al. Engram cell excitability state determines the efficacy of memory retrieval. *Neuron* **101**, 274–284 (2019).
37. Sun, X. et al. Functionally distinct neuronal ensembles within the memory engram. *Cell* **181**, 410–423 (2020).
38. Yuan, A. & Nixon, R. A. Specialized roles of neurofilament proteins in synapses: rpelevance to neuropsychiatric disorders. *Brain Res. Bull.* **126**, 334–346 (2016).
39. Bramham, C. R. & Wells, D. G. Dendritic mRNA: transport, translation and function. *Nat. Rev. Neurosci.* **8**, 776–789 (2007).
40. Choi, J.-H. et al. Interregional synaptic maps among engram cells underlie memory formation. *Science* **360**, 430–435 (2018).
41. Shi, S. H. et al. Rapid spine delivery and redistribution of AMPA receptors after synaptic NMDA receptor activation. *Science* **284**, 1811–1816 (1999).
42. Ostroff, L. E., Fiala, J. C., Allwardt, B. & Harris, K. M. Polyribosomes redistribute from dendritic shafts into spines with enlarged synapses during LTP in developing rat hippocampal slices. *Neuron* **35**, 535–545 (2002).
43. Chung, S. H. et al. Zac1 plays a key role in the development of specific neuronal subsets in the mouse cerebellum. *Neural Dev.* **18**, 25 (2011).
44. Ravasi, T. et al. An atlas of combinatorial transcriptional regulation in mouse and man. *Cell* **140**, 744–752 (2010).
45. Schlisio, S., Halperin, T., Vidal, M. & Nevins, J. R. Interaction of YY1 with E2Fs, mediated by RYBP, provides a mechanism for specificity of E2F function. *EMBO J.* **21**, 5775–5786 (2002).
46. Korb, E., Wilkinson, C. L., Delgado, R. N., Lovero, K. L. & Finkbeiner, S. Arc in the nucleus regulates PML-dependent GluA1 transcription and homeostatic plasticity. *Nat. Neurosci.* **16**, 874–883 (2013).
47. Prickett, A. R. et al. Genome-wide and parental allele-specific analysis of CTCF and cohesin DNA binding in mouse brain reveals a tissue-specific binding pattern and an association with imprinted differentially methylated regions. *Genome Res.* **23**, 1624–1635 (2013).
48. Kinde, B., Wu, D. Y., Greenberg, M. E. & Gabel, H. W. DNA methylation in the gene body influences MeCP2-mediated gene repression. *Proc. Natl Acad. Sci. USA* **113**, 15114–15119 (2016).

Methods

Mice and behavior. As previously described[6], Arc-CreERT2$^+$ mice were bred with R26R-STOP-floxed eYFP homozygous line. Approximately 140 subsequent male offspring were genotyped using the Jackson Laboratory genotyping protocol. Mice were housed 4–5 per cage in a 12-h (06:00–18:00) light/dark colony room at 22 °C with 40–60% humidity. Food and water were provided ad libitum. Behavioral testing was performed during the light phase. One hour before the behavioral test, mice received one dose of 4-hydroxytamoxifen (4-OHT, H6278, Sigma-Aldrich), which opens a ~12-h labeling window[5]. To minimize the nonspecific eYFP label, 1 d before the behavioral task (eg, CFC) mice were single housed in a 24-h dark/dark room. In addition, to reduce anxiety levels, a tube was added to the cage for shelter and nesting. In the next day, mice were injected with TAM 1 h before the CFC. After the behavioral task, mice were either euthanized after 1.5–2 h and brains were collected or placed back into the dark room for the next 48 h. After mice were taken out of the dark, they were returned to a normal 12-h (06:00–18:00) light/dark cycle in the same room. Three days later (total of 5 d after the CFC), half of the mice cohort was euthanized and brains were collected, whereas the other half was returned to the testing room where the mice were exposed to the fear-inducing cue (tone and context). All mouse work was approved by the Committee for Animal Care of the Division of Comparative Medicine at the Massachusetts Institute of Technology

CFC. The CFC apparatus and the acquisition program were from TSE Systems. Mice were introduced into the CFC chamber after 3 min of initial habituation 3-kHz tone with 80-dB intensity was presented for 30 s and was co-terminated with 0.7-mA FS for 1 s. Seventy percent isopropanol was used between experiments to clean the cages. Five days later, mice were introduced into the original conditioned context paired with the tone, and freezing levels were measured for 3 min (TSE software default parameters were used to monitor freezing behaviors) to assess contextual memory. Context B was a modified context A. The stainless steel bars were covered with a white plastic insert; the outer walls of the chambers were covered with shapes of duct tape to change the appearance of the chamber. The chamber was scented with vanilla, the room lighting was much brighter and the mice were transported to the apparatus in a different cart from context A.

Drugs. Recombination in ArcCreERT2 × R26R-STOP-floxed-EYFP transgenic mice was induced using 4-OHT. 4-OHT was dissolved in 2.5 ml of EtOH/100% and rocked on a shaker for 30 min. Next, 5 ml of corn oil was added and rocked on a shaker for 1 h. Finally, tubes were placed for 30 min in 60 °C to allow the full evaporation of EtOH. A single injection of 50 mg kg^{-1} was injected intraperitoneally.

IHC. Mice were transcardially perfused with ice-cold 25 ml of PBS followed by 40 ml of 4% paraformaldehyde in PBS. Brains were removed and post-fixed in 4% paraformaldehyde overnight at 4 °C and transferred to PBS until sectioning. Brains were mounted on a vibratome stage (Leica VT1000S) using superglue and sectioned with the slice thickness of 40 µm. Slices were washed with PBS and blocked using 1% BSA prepared in PBS containing 0.1% Triton-X100 (PBST) for 2 h at room temperature. Blocking buffer was aspirated out, and the slices were incubated with the appropriate primary antibody (Supplementary Table 11) overnight at 4 °C on a shaker. Slices were then washed three times for 15 min each with the blocking buffer and then incubated with Alexa Fluor 488, 594 or 647 conjugated secondary antibodies for 2 h at room temperature. After three washes of 15 min each with blocking buffer and one final wash with PBS for 10 min, slices were mounted with fluromount-G (Electron Microscopy Sciences).

In situ hybridization (RNAscope). Samples were prepared based on the manufacturer's instructions for RNAscope Multiplex Fluorescent v2 Assay (Advanced Cell Diagnostics) with few modifications and combined with the IHC protocol. First, samples were stained for primary (Arc and GFP) and secondary (Alexa Fluor 488 and 594) antibodies (as described in the IHC protocol above). Brain slices were embedded on a glass slide and dehydrated for 30 min at room temperature. Next, a barrier was drawn around each section with the Immedge hydrophobic pen, and samples were treated with RNAscope hydrogen peroxide for 10 min at room temperature (no target retrieval and protease treatment were applied). Per manufacturer's instructions, sections were subjected to probe hybridization (RNAscope Probe- Mm-Gria1, cagalog no. 426241, Advanced Cell Diagnostics), amplification and HRP-C1 signal development using the TSA Plus Cyanine 5 channel.

Imaging analysis. Images were acquired using an LSM 710 or LSM 880 confocal microscope (Zeiss) with ×10, ×20, ×40 or ×63 objectives at identical settings for all conditions. Images were quantified using ImageJ 1.42q or Imarisx64 8.1.2 (Bitplane). For each experimental condition, five coronal sections from at least five animals were used for quantification.

Quantification of tagged cells. The surfaces module was used to detect Arc$^+$ and eYFP$^+$ cells. Double-positive cells (co-localization of Arc$^+$eYFP$^+$) were then counted using the Surface To Surface XTension module. After applying the 'area' filter (>6 µM) to remove unspecific labeling, quantification of the double-positive cells was carried in the CA1, CA3 and DG.

Quantification of Eif and Gria1 proteins/mRNA. The surfaces module was used to detect and 3D render neuron axons based on the GFP signal. EiF2a, Eif4E, Eif3E and Gria1-positive puncta were then counted using the spots module. Finally, the Spots Close To Surface XTension module was run to find the subset of spots that are closer to the surface objects than the defined 1-uM threshold and exclusion of spots that fall outside this range.

Spines morphology. Spines were classified into three types based on the spine length (L), diameter of the head (Dh) and the diameter of the neck (Dn): Stubby spines, Dn = L; Thin spines, L > Dn and Dh ≥ Dn; Mushroom spines, Dh ≥ 2 Dn; and Enlarged mushroom spines, Dh ≥ 2 Dn.

Tissue preparation. Hippocampal tissue was extracted and flash frozen. After extraction, samples were immediately homogenized in 0.5 ml of ice-cold PBS with protease inhibitors (Pi) (11836170001, Roche). To mitigate the sorting effect as much as possible, the suspension was fixed with 1% (for nc-RNAseq/HiC) or 2% (pc-HiC) paraformaldehyde for 10 min, quenched with glycine 2.5 M for 5 min and washed twice with 5 ml of PBS. This process preserves the transcriptional and chromatin landscape and minimizes sorting bias. For ATAC-seq, RNA-seq and capture-HiC, the suspension was centrifuged at 1,200*g* at 4 °C for 5 min, and the pellet was resuspended in 5 ml of NF-1 hypotonic buffer (0.5% Triton X-100/0.1 M sucrose/5 mM $MgCl_2$/1 mM EDTA/10 mM Tris-HCl, pH 8.0, Pi). Next, suspension was dounce-homogenized (pestle A) with 30 strokes, and the pestle was washed with an extra 5 ml of NF-1 buffer for a combined total of 10 ml. The suspensions were collected all in a 15-ml conical tube, filtered with 70-µm mesh filter (08-771-2, Falcon) and incubated on ice for 30 min. Pelleted nuclei (all centrifuges were 4 °C and 1,600*g* for 15 min) were resuspended in 10 ml of PBS+1%BSA+Pi and incubated on ice for 1 h. Nuclei were spun down, and the pellet was resuspended in 1 ml of PBST+1%BSA+Pi and incubated with NeuN, Arc and GFP primary antibodies overnight at 4 °C. Unbound antibodies were washed out twice with 5 ml of PBST and finally resuspended in 1 ml of PBS+1%BSA+Pi and secondary antibodies for 2–4 h at 4 °C. After two washes, nuclei were resuspended in 0.5 ml of PBS+1%BSA+Pi and filtered with a 40-µm mesh filter for fluorescence-activated cell sorting (FACS). DAPI was added directly to the FACS tubes (1:5,000, 10236276001, Sigma-Aldrich).

Flow cytometry. For flow cytometry, nuclei were gated first using forward and side scatter pulse area parameters (FSC-A and SSC-A) excluding debris, followed by exclusion of aggregates using pulse width (FSC-W and SSC-W). Then, isotype control staining was used to set NEUN$^+$, ARC$^+$ and GFP$^+$ gates. To secure a homogeneous neuronal population, the NeuN$^+$ population was gated before gating populations based on ARC$^+$ and GFP$^+$ fluorescence. We sorted four different populations from three different time points: approximately 1.5–2 h after exposure to FS (1) NeuN$^+$GFP$^+$ and (2) NeuN$^+$GFP$^-$; after 5 d, in the absence of retrieval, we collected (3) NeuN$^+$GFP$^+$; and, in a different cohort, mice were re-exposed to the conditioned stimulus, and, 1.5–2 h after re-exposure, we collected (4) NeuN$^+$ARC$^+$GFP$^+$. All nuclei were sorted into 1.5-ml Eppendorf tubes containing 500 µl of PBS+1%BSA+Pi for ATCA-seq; 200 µl of digestion buffer (RecoverAll Total Nucleic Acid Isolation Kit for FFPE, cat. AM1975, Invitrogen) for RNA-seq; and 500 µl of fresh ice-cold lysis buffer (10 mM Tris, pH 8, 10 mM NaCl, 0.2% IGEPAL CA-630, Pi and PCR-grade water) for Hi-C/capture-HiC. Data analysis was performed with FlowJo software (v10).

ChIP-qPCR. Immediately after sorting, 10,000 cells were pelleted at 4 °C and 1,600*g* for 15 min and re-suspended in SDS lysis buffer. ChIP was conducted per the manufacturer's instructions for the ChIP-IT High Sensitivity Kit (cat. no. 53040, Active Motif) using anti-H3K4me1 (Abcam, ab8895, 1:100) and anti-H3K27ac (Abcam, ab4729, 1:100) antibodies. ChIP assays were performed in a Bio-Rad CFX96 connect real-time PCR unit using SsoFast EvaGreen qPCR reagent mix (Bio-Rad, 172-5202). Samples were assayed in triplicate, and results were normalized to input. Sequences of primer pairs for ChIP-qPCR assays are listed in Supplementary Table 12.

ATAC-seq. *Libraries preparation.* ATAC-seq libraries were prepared as previously described[49] with minor modifications. Ten thousand cells from each group were pulled from 8–10 different mice and considered as $n=1$. Then, 3–4 biological replicates ($n=3$–4) were used for library preparation. Immediately after sorting, cells were spun down (4 °C at 1,600*g* for 15 min) and resuspended in fresh 50 µl of cold lysis buffer (0.15% NP-40 instead of IGEPAL) and rocked on ice for 10 min. Next, tagmentation reaction (Nextera DNA Sample Prep Kit, 24 reactions, FC-121-1030, Illumina) was carried out in 25 µl of volume (12.5 µl of TD, 1.25 µl of TDE1 and 11.25 µl of nuclease-free water) for 30 min at 37 °C with gentle rocking. Tagmented DNA fragments were amplified and barcoded using PCR reaction (1 cycle, 5 min at 72 °C and 30 s at 98 °C; 10 cycles, 15 s at 98 °C, 30 s at 60 °C and 3 min at 72 °C). Following the manufacturer's protocol, amplified DNA was cleaned and purified using 1.8× AMPure beads (AMPure XP beads, Beckman Coulter,

A63880). After bioanalyzer quality control for library size and distribution, libraries were sequenced on the Illumina NextSeq 550 platform at the MIT BioMicro Center.

ATAC-seq analysis. The raw fastq data of 40-bp paired-end sequencing reads were aligned to the mouse mm9 reference genome using Bowtie 2.0 in paired-end mode[50]. The Samtools collection[51] was used to sort, remove PCR duplicates (rmdup), index BAM files (index) and calculate library statistics (flagstat; Supplementary Table 13). BAM files were downsampled from properly aligned, paired and unique reads to 50 M. Open chromatin peaks were analyzed using MACS2 (ref. [52]) software. DARs were identified by Diffbind v1.16.3 (ref. [53]) with default parameters and settings to use DESeq2 (cutoff; false discovery rate (FDR) < 0.01; FCs > 1.5). Full matrix of normalized counts (RPKM[54]) was retrieved by the DiffBind package. For generation of bigwig tracks, pileup signal files (fragment pileup per million reads) in bedGraph format were constructed by using the MACS2 callpeak function with the -B –SPMR flags. Then, normalized FE over input lambda tracks were generated using the bdgcmp function of MACS2 with the setting -m FE. Then, bedGraph files were converted to bigwig format.

IGV[55] tools were used for visualization of bigwig files. ChromHMM[56] was used to establish a chromatin state model from two independent studies that used bulk hippocampus tissue before and after FS[21,22] and to determine FE of DARs over the state model. Motif enrichment analysis[57,58] and peaks annotation were performed by HOMER[59] tools. All codes are available in the Supplementary Software File.

RNA-seq. *RNA extraction and library preparation.* Immediately after fixation and sorting (see 'Tissue preparation'), 4 ul of protease was added to digestion buffer (RecoverAll Total Nucleic Acid Isolation Kit for FFPE, Life Technologies, AM1975). Samples were incubated in heat blocks for 15 min at 50 °C and then for 15 min at 80 °C. Next, 0.75 ml of Trizol LS (TRIzol LS Reagent, Thermo Fisher Scientific, 10296028) and 0.2 ml of phenol:chloroform solution (phenol:chloroform:isoamyl alcohol, 1 Phase, VWR International, K169) was added to each sample followed by vigorous shaking for 5 min at room temperature. Suspension was placed into Phase Lock Gel heavy tubes (5 Prime, 2302830) and spun down at 13,000 r.p.m. for 5 min. Aquatic phase with nucleic acids was extracted from the tubes to fresh Eppendorf tubes with equal amounts of ethanol 100%. RNA purification was carried by Direct-zol RNA Microprep Kit (Zymo Research, R2060) for RNA purification according to the manufacturer's instructions. RNA was eluted (10 ul, DEPC) and then stored at −80 °C. SMARTer Stranded Total RNA-Seq Kit v2-Pico Input Mammalian (Clontech, 635006) was used for the library preparation and amplification. Three biological replicates were used for library preparation. Libraries were prepared according to the manufacturer's instructions with no extra fragmentation step (FFPE, option 2; see manual), with depletion of ribosomal complementary DNA and final PCR amplification (15 cycles). Libraries were sequenced on the Illumina HiSeq 2000 platform at the MIT BioMicro Center.

RNA-seq analysis. The raw fastq data were aligned to the mouse mm9 reference genome using Bowtie 2.0. The mapped reads from gene bodies (including exon and intron reads) were processed by Cufflinks 2.2 (ref. [60]) and DEseq2 (ref. [61]) with UCSC mm9 reference gene annotation to estimate transcript abundances. Differential gene expression and downstream analyses were performed using DEseq2 and custom R scripts. Relative abundance of transcripts was measured by fragments per kilobase of exon per million fragments mapped.

For the analysis of transcriptional programs, the expression of each gene was assessed for different memory phases (Activated-early, Activated-late and Reactivated) by their $\log_2$FC from the basal state. One thousand ninety-five DEGs passed the cutoff criteria, in which we observed at least in one comparison of P value of < 0.01 and $\log_2$FC > 1. Then, genes were unbiasedly clustered by the k-means function in R.

Hi-C. Nuclei from fixed cells (see 'Tissue preparation') were sorted into 1.5-ml Eppendorf tubes containing 500 µl of fresh ice-cold lysis buffer (10 mM Tris, pH 8, 10 mM NaCl, 0.2% IGEPAL CA-630, Pi and PCR-grade water) and frozen on dry ice and stored at −80 °C until they were used. Hi-C libraries were prepared from 100,000 cells per group (collected from two animals) in two biological replicates using the Dovetail Hi-C Kit manual (v.1.03, Dovetail Genomics). The six Hi-C libraries were sequenced (paired-end) on an Illumina NextSeq 500 platform. The HOMER Hi-C pipeline was used to filter experimental artifacts, such as circularization, self-ligations and PCR duplicates. Filtered reads were aligned to the reference mouse genome (mm9) and further processed using the HOMER HI-C pipeline.

HOMER's Hi-C tools were used to perform principal components analysis (PCA) on the Hi-C data to identify sub-nuclear compartments (A and B) at 50-kb resolution (Supplementary Software). For the compartment switch analysis, we first subtracted the PC1 values between the groups. Next, we identified the top B-to-A transitions as regions with PC1 change above the 90th percentile and the top A-to-B transitions as regions with PC1 change below the 10th percentile. Because sub-nuclear compartments are regulated as units of several hundred kilobases, we consolidated consecutive 50-kb A-to-B or B-to-A segments that were within a distance of 100 kb of each other. Consolidated domains that were less than 200 kb in total size were discarded. Compartment switches were considered only if a negative value was transformed to a positive value (and vice versa). Finally, positive and negative values of the first component were compared among all three populations of neurons (Basal, Activated-early and Activated-late).

pc-HiC. After fixation and sorting (see 'Tissue preparation'), cells were sorted into 1.5-ml Eppendorf tubes containing 500 µl of fresh ice-cold lysis buffer (10 mM Tris, pH 8, 10 mM NaCl, 0.2% IGEPAL CA-630, Pi and PCR-grade water), frozen on dry ice and stored at −80 °C until they were used. Hi-C libraries were prepared from 10,000 cells per group (n = 3–4), as previously described[62], with some modifications. Samples were spun down (4 °C at 1,600g for 20 min), and the pellet was resuspended in 400 µl of 1.2× CutSmart Buffer (New England Biolabs). The first restriction digestion was carried out as described in the original protocol with 1,500 U of HindIII (R3104L, New England Biolabs) as the six-base cutter (instead of BglII in the original protocol). After Biotin labeling and overnight ligation (see the original protocol for details), samples were spun down (4 °C at 1,600g for 15 min), and the pellet was resuspended in 25 µl of PBS. The suspension was incubated at 65 °C with 3 µl of proteinase K for 12–16 h. Purification of Hi-C DNA was carried out as described in the original protocol with 100 µl of streptavidin beads (Dynabeads M-280-streptavidin, Life Technologies, 11205D). For the second restriction enzyme, we used the four-base cutter Hpych4V (10 U per sample, R0620S, New England Biolabs). After the A-tailing reaction (see the original protocol for details), samples were amplified using PCR (17 cycles) and purified with AMPure XP beads. Hi-C libraries were eluted in 20 ul of 10 mM Tris-HCl (pH 8.5). Bait capture system design for pc-HiC A List of 5,000 mouse gene promoters was obtained from the previously published protocol in Schoenfelder et al.[29]. The list contains only transcripts with a biotype of protein-coding regions with HindIII restriction fragment sites. Two 120-bp capture probes were designed, one to each end of the fragment. The probes were synthesized by Agilent Technologies according to the SureSelect Target Enrichment System (Agilent Technologies).

pc-HiC library preparation and sequencing—To capture Hi-C ligation products containing promoter sequences, we used the previously published protocol[29]. Briefly, hybridization blockers (Agilent Technologies) were added to the Hi-C DNA libraries. Hybridization buffer and capture bait RNA were prepared according to the manufacturer's instructions (SureSelect Target Enrichment System, Agilent Technologies). Next, the Hi-C library DNA/hybridization blockers were heated for 5 min at 95 °C before lowering the temperature to 65 °C. Hi-C library DNA was mixed with hybridization buffer (pre-warmed for 5 min to 65 °C) and subsequently with the custom-designed capture bait system (pre-warmed for 3 min to 65 °C), consisting of 10,000 biotinylated RNAs targeting the HindIII restriction fragment ends of 5,000 mouse gene promoters (Agilent Technologies; see Supplemental Material for capture bait design). After 24 h at 65 °C in the PCR machine, biotin pulldown (MyOne Streptavidin T1 Dynabeads, Life Technologies) and washes were performed following the SureSelect Target Enrichment System protocol (Agilent Technologies). After the final wash, beads were resuspended in 30 µl of NEBuffer 2 without prior DNA elution, and a post-capture PCR (four amplification cycles using Illumina universal primers) was performed on DNA bound to the beads via biotinylated RNA. pc-HiC libraries were paired-end sequenced (NextSeq 500, Illumina).

pc-HiC analysis—The HiCUP pipeline[63] was employed to process the raw fastq sequencing reads. This pipeline was used to map the read pairs against the mouse (mm9) genome, to filter experimental artifacts (such as circularized reads and re-ligations) and to remove duplicate reads. For the pc-HiC data, the resulting BAM files were downsampled and processed using CHiCAGO version 1.2.0 (ref. [64]) following the default settings to call significant interactions. The full details of this pipeline are available from Babraham Bioinformatics (http://www.bioinformatics.babraham.ac.uk/).

Stereotaxic AAV injection. ArcCreERT2 mice were anaesthetized with avertin for AAV9-EF1a-DIO-hChR2-EYFP (serotype 5, obtained from the UNC Vector Core) virus infusion. First, a small hole was made in the skull above the dorsal hippocampus (relative to bregma: anterior–posterior, −2.0, and medio–lateral, ±1.5); a Hamilton syringe with 33-gauge needle was lowered to −1.8 DV; and 500 nl of virus was infused with a flow rate of 50 nl per minute into both hippocampi. The needle was withdrawn after a 10-min post-injection period, and mice were allowed to recover for 4 d.

Statistical analysis. For nRNA-seq, ATAC-seq, pc-HiC and Hi-C experiments, no statistical methods were used to predetermine sample sizes, but our sample sizes were similar to those reported in similar publications[13,20,21,27,29,37]. In addition, in these experiments, sample size was estimated according to data variance between biological replicates and distance to control condition (Basal group). No statistical methods were used to predetermine sample sizes in 3C and ChIP-qPCR experiments. Sample sizes were chosen based on previous literature using similar experimental paradigms[65]. For all other experiments, sample size was calculated by power analysis (http://www.lasec.cuhk.edu.hk/sample-size-calculation.html) to estimate the number of replicates required assuming a 5% significance level. All measurements were taken from distinct samples, and the same sample was never measured repeatedly.

Values are presented as dot plots with individual data points, violin plots or boxes and whiskers with mean interquartile range, the minimum, maximum

and ±s.e.m. as indicated in the figure legends. Statistical analyses were designed using the assumption of normal distribution, although that assumption was not explicitly tested. Statistical comparisons included Pearson's correlation (parametric, two-sided), Student's *t*-test (two-sided, unpaired), one- or two-way analysis of variance (ANOVA), followed by Dunnett's or Bonferroni's multiple comparison post hoc tests (as specified in the figure legends). *P* values < 0.05 were considered statistically significant (unless $\log_2$FC criteria were also considered, as specified in the figure legends or main text).

Statistical significance of differences between groups was analyzed using the following software and statistical tests: 1) differential peaks analysis: Diffbind (v2.10); 2) significant interaction analysis: CHiCAGO (v1.2.0); 3) differential gene analysis: DESeq2 v.1.22.2; 4) statistical analyses for motif and annotation enrichment: HOMER (v4.1); and 5) other software for data and statistical analysis: R Studio (v3.5.2) and R packages ggplot2 (v3.1.0), circlize (v0.4.5), ComplexHeatmap (v1.2.0), gridExtra (v2.3), GeneOverlap (v1.18.0) and bedr (v1.0.6); GraphPad Prism (v8.2.1); Microsoft Excel; ChromHMM (v1.15); Bedtools (v2.25.0); DeepTools (v3.2.1); IGV (v2.3); and Washu browser (v50.3.6).

Reproducibility. TRAP mice (n = ~140) with the same age (~90 d) and sex (males) were raised in the same conditions and randomly allocated to the different experimental groups. Blinding was not applied in the behavioral studies (CFC) and imaging acquisition because animals and samples need to be controlled by treatment or conditions. Individuals generating the next-generation sequencing data were blinded to the outcome measures. Individuals performing the imaging quantification analysis for Eif, Gria1 proteins/mRNA and spine morphology were blinded to the groups. All IHC and FACS experiments were repeated independently with similar results.

Accession codes. Raw and processed data sets generated during this study are available in the Gene Expression Omnibus repository using accession number GSE152956.

* SubSeries that are linked to GSE152956:
https://www.ncbi.nlm.nih.gov/geo/query/acc.cgi?acc=GSE152775
https://www.ncbi.nlm.nih.gov/geo/query/acc.cgi?acc=GSE152953
https://www.ncbi.nlm.nih.gov/geo/query/acc.cgi?acc=GSE152954
https://www.ncbi.nlm.nih.gov/geo/query/acc.cgi?acc=GSE152955

Data availability

Supplementary Tables 1–11 provide direct access to the main results derived from the transcriptome and epigenome assays presented in this study. In addition, raw and processed data sets generated during the study are available in the Gene Expression Omnibus repository using the accession number GSE152956. Any other data that support the findings of this study are available from the corresponding author upon reasonable request.

Code availability

Codes used for the analysis of this study are available in the supplementary software appendix. A live version of the custom R scripts generated during this study is available in the Github repository at https://github.com/vishnudileep2000/IntronVsExon_RNAseq

References

49. Buenrostro, J. D., Giresi, P. G., Zaba, L. C., Chang, H. Y. & Greenleaf, W. J. Transposition of native chromatin for fast and sensitive epigenomic profiling of open chromatin, DNA-binding proteins and nucleosome position. *Nat. Methods* **10**, 1213–1218 (2013).
50. Langmead, B. & Salzberg, S. L. Fast gapped-read alignment with Bowtie 2. *Nat. Methods* **9**, 357–359 (2012).
51. Li, H.et al. The Sequence Alignment/Map format and SAMtools. *Bioinformatics* **25**, 2078–2079 (2009).
52. Zhang, Y.et al. Model-based analysis of ChIP-Seq (MACS). *Genome Biol.* **9**, R137 (2008).
53. Stark, R. & Brown, G. DiffBind: differential binding analysis of ChIP-Seq peak data.https://doi.org/10.18129/B9.bioc.DiffBind(2011).
54. Robinson, M. D. & Oshlack, A. A scaling normalization method for differential expression analysis of RNA-seq data. *Genome Biol.* **11**, R25 (2010).
55. Thorvaldsdóttir, H., Robinson, J. T. & Mesirov, J. P. Integrative Genomics Viewer (IGV): high-performance genomics data visualization and exploration. *Brief. Bioinform.* **14**, 178–192 (2013).
56. Ernst, J. & Kellis, M. Chromatin-state discovery and genome annotation with ChromHMM. *Nat. Protoc.* **12**, 2478–2492 (2017).
57. Benner, C., Heinz, S. & Glass, C. K. HOMER: software for motif discovery and next generation sequencing analysis http://homer.ucsd.edu/ (2017).
58. Schep, A. N. et al. Structured nucleosome fingerprints enable high-resolution mapping of chromatin architecture within regulatory regions. *Genome Res.* **25**, 1757–1770 (2015).
59. Heinz, S.et al. Simple combinations of lineage-determining transcription factors prime cis-regulatory elements required for macrophage and B cell identities. *Mol. Cell* **38**, 576–589 (2010).
60. Trapnell, C.et al. Differential gene and transcript expression analysis of RNA-seq experiments with TopHat and Cufflinks. *Nat. Protoc.* **7**, 562–578 (2012).
61. Robinson, M. D., McCarthy, D. J. & Smyth, G. K. edgeR: a Bioconductor package for differential expression analysis of digital gene expression data. *Bioinformatics* **26**, 139–140 (2009).
62. Nagano, T. et al. Single-cell Hi-C for genome-wide detection of chromatin interactions that occur simultaneously in a single cell. *Nat. Protoc.* **10**, 1986–2003 (2015).
63. Wingett, S. W. et al. HiCUP: pipeline for mapping and processing Hi-C data. *F1000Research* **4**, 1310 (2015).
64. Cairns, J. et al. CHiCAGO: robust detection of DNA looping interactions in Capture Hi-C data. *Genome Biol.* **17**, 1–17 (2016).
65. Kagey, M. H. et al. Mediator and cohesin connect gene expression and chromatin architecture. *Nature* **467**, 430–435 (2010).

Acknowledgements

We thank E. Niederst, J. Penney, S. Barker, R.T. Stott, M. Victor, A. Watson, N. Dedic, E. Lockshin and the members of the L.-H.T. Lab for helpful discussion and suggestions. We thank lab manager Y. Zhou and E. McNamara for mice colony maintenance. We thank P. Autissier (Whitehead Institute) for help with FACS. This work was supported by National Institutes of Health (NIH) grants RF1AG062377, AF1AG054012, RO1NS102730 and RF1AG064321, the JPB Foundation, the Alana Foundation, the LuMind Down Syndrome Foundation, the Cure Alzheimer's Fund CIRCUITS consortium and the Robert A. and Renee E. Belfer Family Foundation to L.-H.T. This work was also supported, in part, by NIH grants R01AG058002, U01NS110453, R01AG062335 and UG3NS115064 to M.K. and L.-H.T. and R01AG067151, R01MH109978, U01MH119509, R01HG008155 and U24HG009446 to M.K. V.D. is supported by the AARF-19-618751 grant from the Alzheimer's Association. H.S.M. is supported by the Burroughs Wellcome Fund and a UNCF–Merck postdoctoral fellowship. C.A. is supported by the JPB Foundation. R.M.R. is supported by NIH T32 grant 5T32HD09806. The Hi-C libraries preparation kit was received as a generous gift from DovetailTM (v.1.03, Dovetail Genomics). We thank the Dovetail team for helpful discussion and suggestions.

Author contributions

A.M. and L.-H.T. conceptualized and designed the project. A.M. and A.Z. performed behavioral experiments, ISH, immunostainings and IMARIS analysis. C.A. performed virus injection and immunostainings. A.M. and H.S.M. performed ATAC-seq experiments. A.M. and A.Z. performed nRNA-seq experiments. A.M., H.S.M. and V.D. performed pc-HiC and Hi-C experiments. A.M., H.S.M., V.D., R.M.R. and J.D.V. performed ATAC-seq analysis. A.M., R.M.R., H.S.M., V.D. and F.G. performed nRNA-seq analysis. A.M., V.D., H.S.M. and R.M.R. performed pc-HiC and Hi-C analysis. All authors helped interpret the data. A.M., H.S.M., V.D., R.M.R., J.Z.Y., M.K. and L.-H.T. wrote the manuscript with the input from all authors. L.-H.T. provided the tools and supervised the project.

Competing interests

The authors declare no competing interests.

Additional information

Extended data is available for this paper at https://doi.org/10.1038/s41593-020-00717-0.

Supplementary information is available for this paper at https://doi.org/10.1038/s41593-020-00717-0.

Correspondence and requests for materials should be addressed to A.M. or L.-H.T.

Reprints and permissions information is available at www.nature.com/reprints.

Peer review Information *Nature Neuroscience* thanks Kaoru Inokuchi, Hongjun Song, and Jason Stein for their contribution to the peer review of this work.

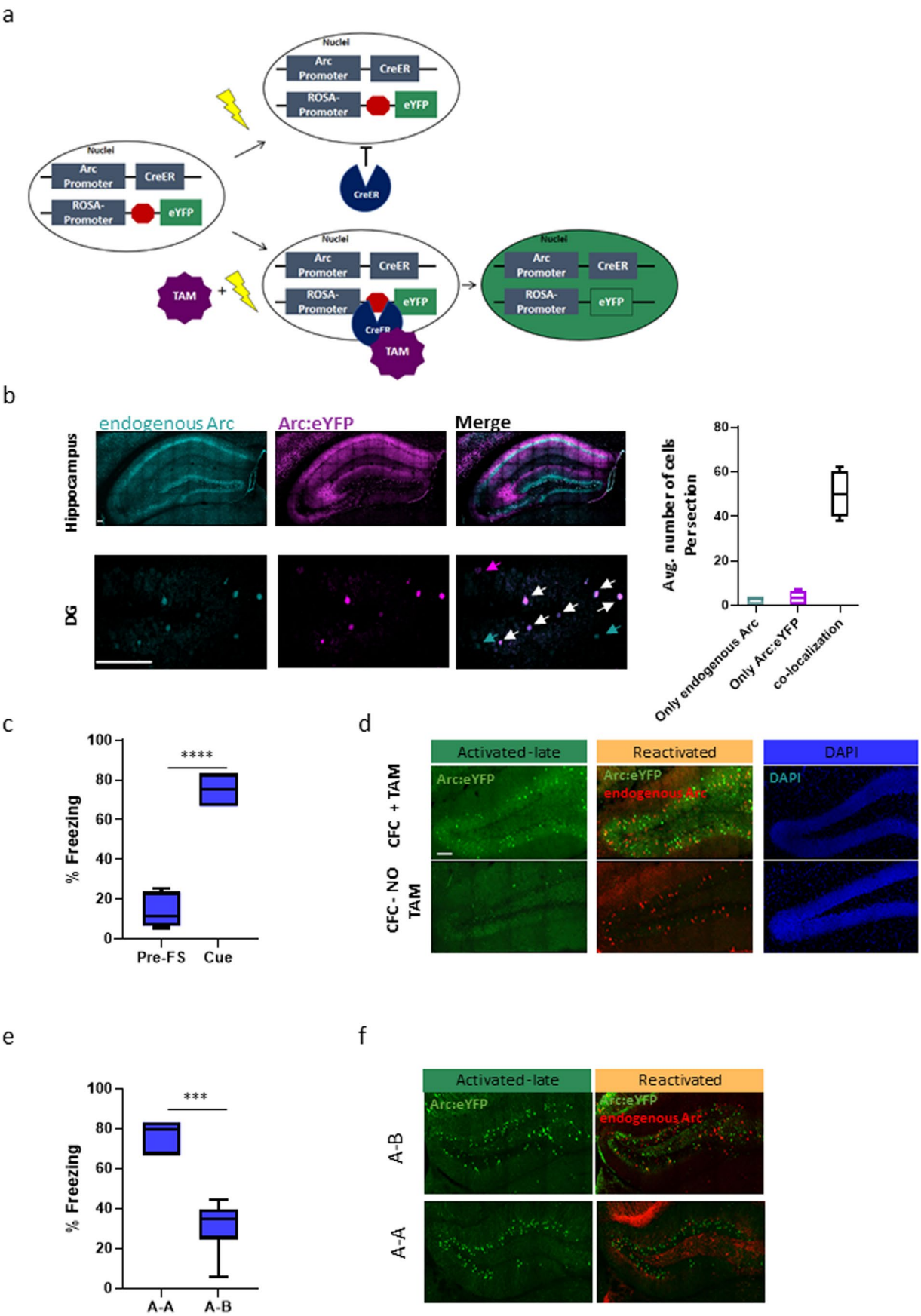

Extended Data Fig. 1 | See next page for caption.

Extended Data Fig. 1 | Reactivated cells play a key role in encoding prior experience. a, Schematic of the Targeted Recombination in Active Populations (TRAP), which requires two transgenes, one that expresses CreERT2 from an activity-dependent Arc promoter (ArcCreERT2) and one that allows expression of the eYFP reporter, in a Cre- dependent manner. Administration of TAM to TRAP mice results in a permanent eYFP label in the initially activated Arc neurons. Without TAM, CreERT2 is retained in the cytoplasm of active neurons in which it is expressed, so no recombination can occur. **b**, Representative images and co-localization analysis between endogenous Arc protein (Cyan) and the Arc:eYFP reporter (Magenta), 1.5 h after the FS. Upper panel shows images from the whole hippocampus and lower panel images shows neurons from the DG. Magenta arrows—neurons with only Arc:eYFP reporter signal, Cyan arrows—neurons with only endogenous Arc signal, White arrows—neurons with signal from both populations. Analysis was performed using IMARIS module (co-localization tools) and revealed an average of 84% overlap between the two populations. Scale bar, 100 μm. n = 3 mice /5 slices per animal, boxplot indicates the mean, interquartile range and the minimum and maximum. **c**, Contextual fear conditioning (CFC) freezing test. Percentage of the time freezing levels were measured during habituation (Day 0, Pre-FS) and during the re-exposure (Day 5) to the fear-inducing cue. n = 30 mice, boxplot indicates the mean, interquartile range and the minimum and maximum, two-sided unpaired Student's t-test, t = 15.63, df=16, ****P < 0.0001. **d**, Representative images of Activated -late and Reactivated neurons in the hippocampus in two experimental groups; CFC with (TAM) or without (NO-TAM) tamoxifen administration. Scale bar, 100 μm. **e**, Contextual fear conditioning (CFC) freezing test. Percentage of the time freezing levels were measured during the re-exposure to the fear inducing cue (A-A) and during the exposure to a novel neutral environment (context B). n = 15 mice, boxplot indicates the mean, interquartile range and the minimum and maximum, two-sided unpaired Student's t-test, t = 8.506, df=14, ****P < 0.0001. **f**, Representative images of Activated -late and Reactivated neurons from the DG in the A-A' or A-B group.

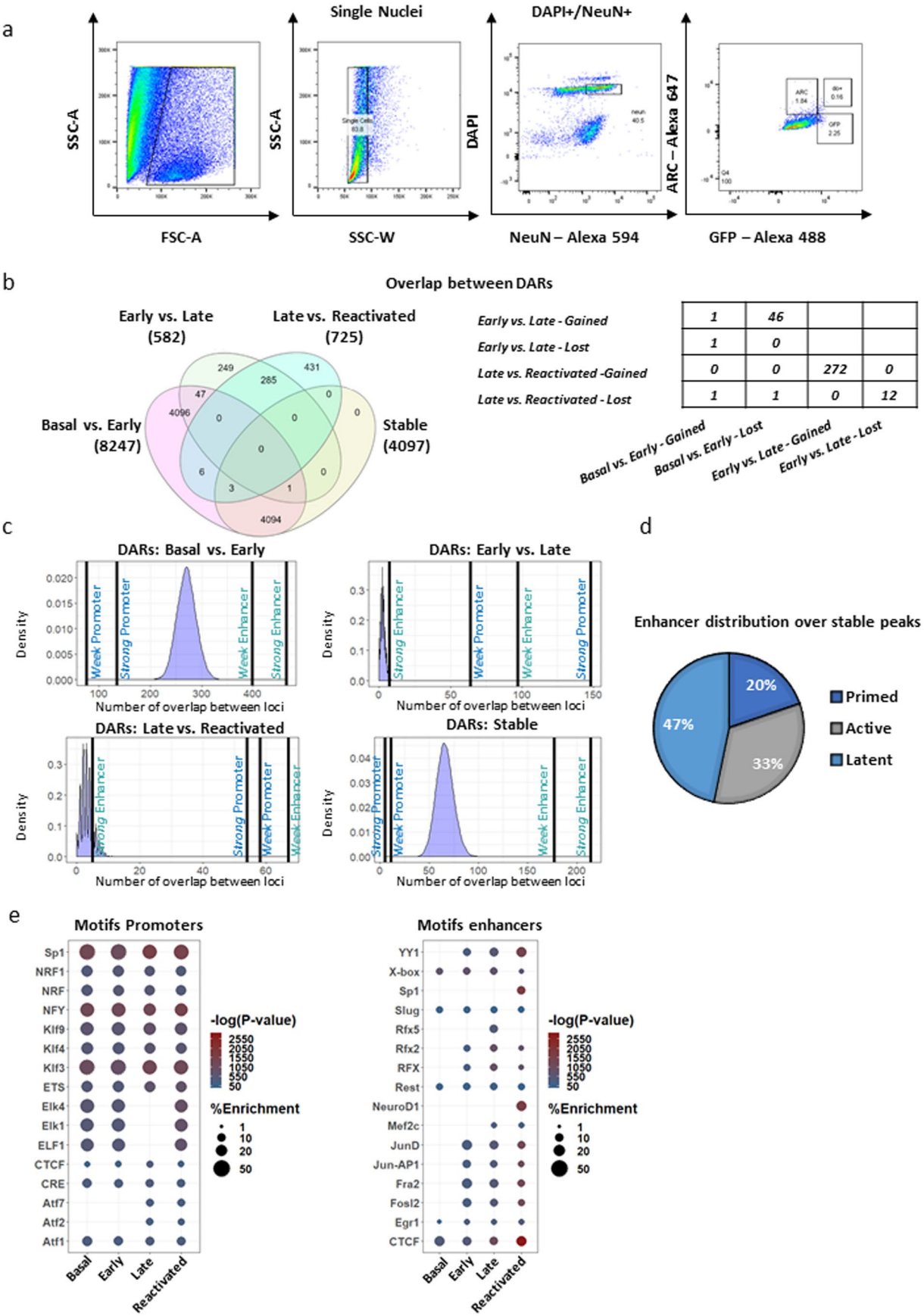

Extended Data Fig. 2 | See next page for caption.

Extended Data Fig. 2 | Stable DARs are predominantly enriched for enhancers marks. a, Workflow for the flow cytometry dissection of different neuronal population from the hippocampus, during memory formation and retrieval. Representative FACS plots showing expression of all population (left panel). Further selection was made on single nuclei and NeuN + /DAPI + population (middle panel). Last, selection was made on the gated sub-population; GFP + (adjusted to ~2.5% from all cells), ARC + /GFP + (~0.15% from all cells) and nuclei were sorted to 1.5 ml Eppendorf tubes coated with 200ul of 1% PBS. **b**, Venn Diagram (left) and table (right), which illustrate the overlap between the DARs identified in the different pairwise comparisons during memory formation and recall. **c**, Resampling-based statistical analysis was performed to determine if the enrichments of chromatin states over ChromHMM emissions (observed) are statistically significant. Expected enrichment was calculated by performing 10,000 randomized sets of overlaps (permutations) between 'all accessible sites' and 'all histone modifications sites (that is all emissions)' and presented as histogram in the figure. Sample size of each randomized set was determined by the size of DARs from each state. The mean and standard deviation of the sample was calculated (Supplementary Table 3). The number of observed overlaps between DARs and each emission was calculated and presented as lines. z-score was calculated as fallows; $Z = (\text{observed values } (X) - \text{mean of the sample } (\mu))/(\text{standard deviation of the sample } (\sigma))$. z-score Basal vs. Early; S.E 10.5, W.E 6.9. Stable; S.E 16.9, W.E 12.7, all $p < 0.0001$, z-score Early vs. Late; S.P 91.7, W.P 38.7. Late vs. Reactivated; S.P 26.8, W.P 28.9, all $p < 0.0001$. p-values (Two-Sided) were calculated from z-table. Full analysis is reported in Supplementary Table 3. **d**, Pie chart shows percentage of different enhancer states, for all stable regions. Overlap of each individual stable region was performed with previously published H3K4me1 and H3K27ac ChIP-seq data, obtained 1h after FS 29[21]. Enhancers states were classified as 'primed'—overlap with regions marked with only H3K4me1, 'active'—with H3K4me1/H3K27ac or 'latent'—no overlap. **e**, Motifs identified from nucleosome free regions (NFR) on the ATAC-seq tracks from each state (Basal, Activated-early, Activated-late and Reactivated). Peaks were divided into positions that annotated to promoters (5 kb from TSS) and enhancers (>5 kb from TSS). Circle size indicate percentage of enrichment (1–50%). Color indicates –log(*P*-value).

a

	Basal	Early	Late	Reactivated
Number of significant interactions	18542	18990	19168	19687
Number of captured baits	4171	3677	4022	4021
Mean number of significant interactions per bait	4.44	5.16	4.76	4.89

b

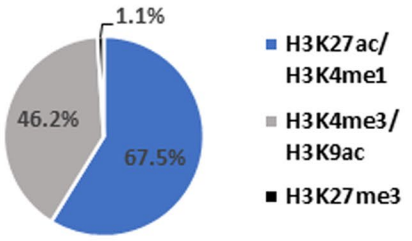

c

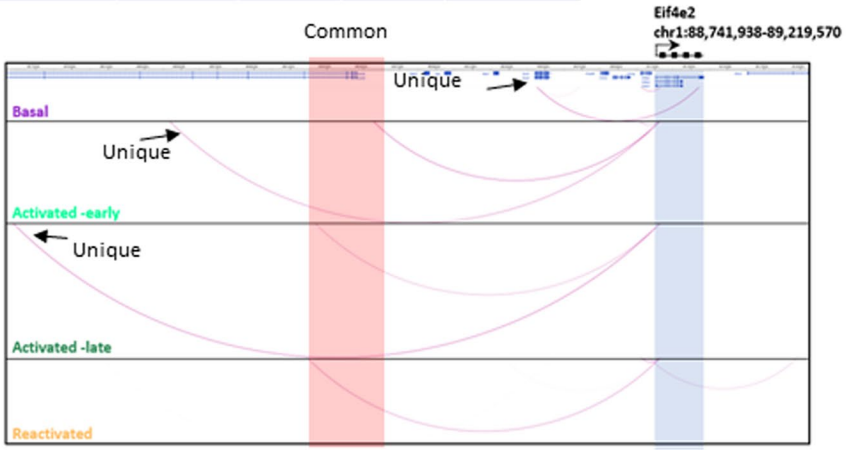

d

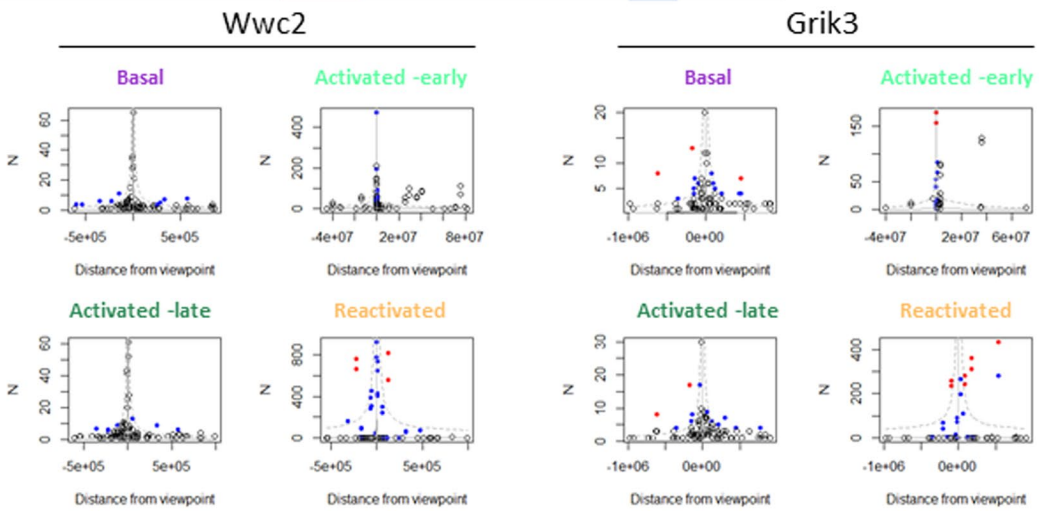

e

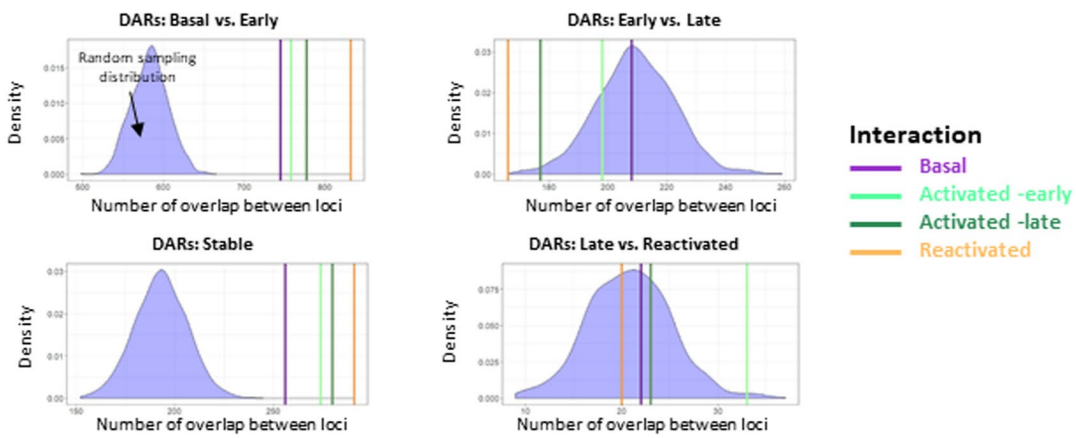

Extended Data Fig. 3 | See next page for caption.

Extended Data Fig. 3 | Coordinated priming of the epigenetic state during memory encoding and consolidation facilitates long-range interactions during reactivation. a, The properties of CHiCAGO-detected interactions in each phase (Basal, Activated -early, Activated -late and Reactivated). Default settings and a score threshold of 5 were used in significant interaction calling, performed jointly on all replicates. **b**, Pie chart represent the percentage of all CHiCAGO-detected interactions that are demarcated by either H3K27ac/H3K4me1 (67.5% enhancers marks), H3K4me3/H3K9ac (46.2% promoters mark) or H3K27me3 (1.1% repressive marks). **c**, WashU epigenome browser image, encompassing ~ 500 Kb region around the Eif4e2 genes. Arcs shows significant common (red rectangle) and unique (arrowed) enhancers that interacts with promoters (blue rectangle). **d**, Examples of interactions called by CHiCAGO. Plots showing all the read counts from bait-other-end (enhancer), within 500–700 kb (upstream and downstream) of the Grink3 and Wwc2 promoters. Significant interactions detected by CHiCAGO (score ≥5) are shown in red, and sub-threshold interactions (3 ≤ score < 5) are shown in blue. Grey lines show expected counts and dashed lines the upper bound of the 95 % confidence intervals. **e**, Overlap enrichment analysis between interacting enhancers and DARs, using a permutation procedure on 10,000 randomized sets of accessible sites. Histogram present random sampling distribution of accessible sites for each condition (Basal vs. Activated-early, Activated-early vs. Activated-late, Activated-late vs. Reactivated, Stable). The number of overlapped loci is presented in colored lines from Basal, Activated-early, Activated-late and Reactivated neurons. DARs of BAS vs. Activated-early (z-score; 7.1, 7.7, 8.5, 10.9). DARs of Activated-early vs. Activated-late (z-score; −0.1, −0.8, −2.4, −3.2). DARs of Activated-late vs. Reactivated (0.4, 1.8, 0.4, −0.2). DARs of stable (z-score; 1.7, 2.0, 6.5, 7.3).

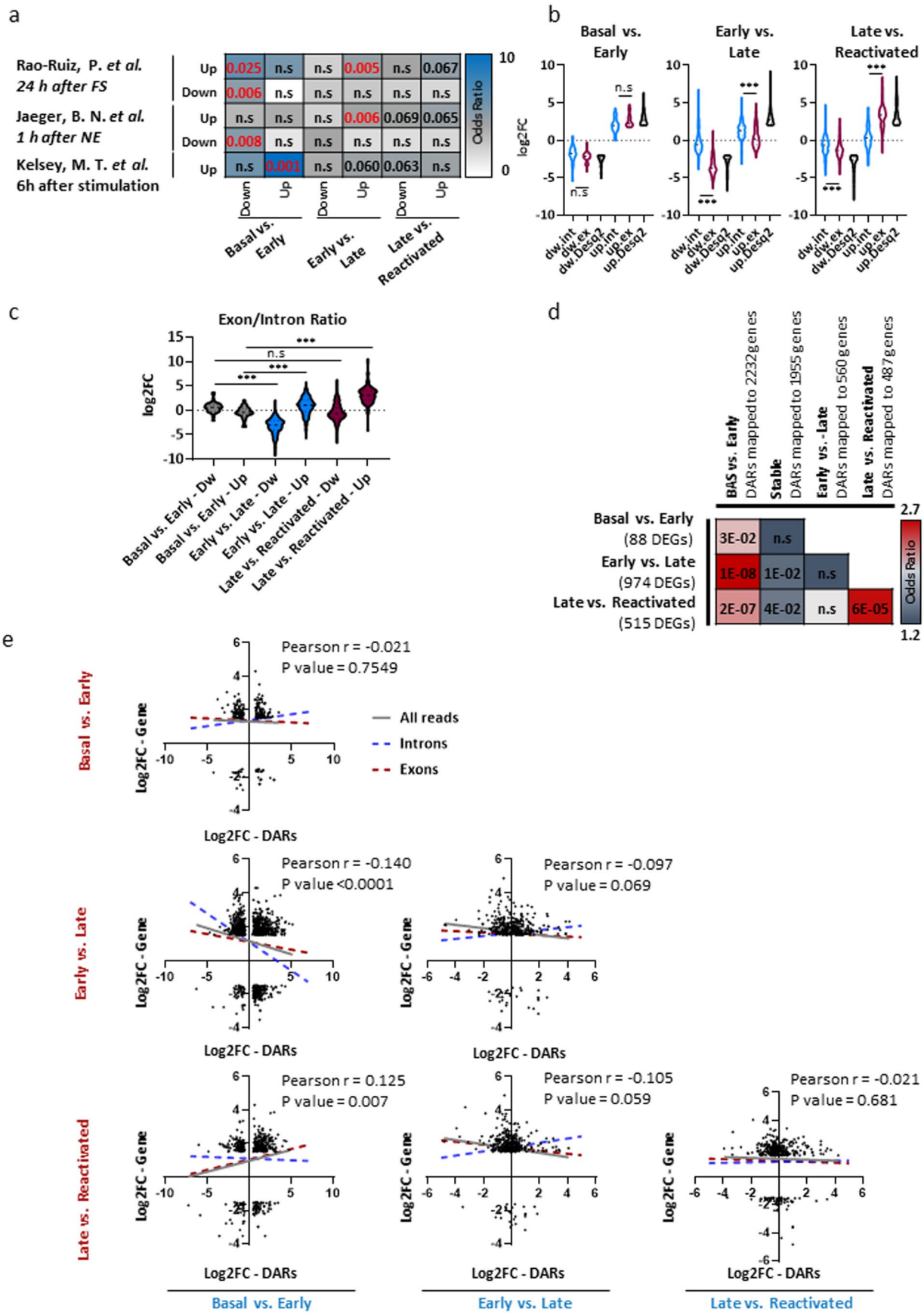

Extended Data Fig. 4 | See next page for caption.

Extended Data Fig. 4 | Chromatin changes that occur during the early phase enable transcriptional changes observed at a later time point, primarily in reactivated engram cells. a, Overlap analysis between gene names from the pair-wise differential analysis and previously published data of: i) activated DG granule cells 1 h after novel exposure[32] ii) 24 h after FS[20] and iii) after prolonged stimulation (6 h) of mouse cultured cortical neurons with KCl[33]. Analysis was carried by GeneOverlap R package. **b**, Exonic (red) and intronic (blue) reads were quantified separately across all conditions and compared to transcriptional activity as measured by DEseq2. Reads were normalized (RPKM) and the log2FC changes are presented for each state. Violin plot indicates the mean, interquartile range and the minimum and maximum, one-way ANOVA (parametric, unpaired), Basal vs. Early; $F(5, 248) = 389.9$. Early vs. Late; $F(5, 2374) = 2183$. Late vs. Reactivated. $F(5, 1357) = 945.5$, All Ps < 0.0001. Bonferroni's multiple comparisons. n.s = not significant, ***P < 0.0001. **c**, Exon/Intron ratios were measured in each cluster across all conditions (Log2FC scale). Violin plot indicates the mean, interquartile range and the minimum and maximum, one-way ANOVA (parametric, unpaired), $F(5, 1143) = 260.2$, P < 0.0001. Bonferroni's multiple comparisons test. n.s = non-significant, ***P < 0.0001. **d**, Overlap analysis between DARs and DEGs during different memory phases. DARs on Intergenic and introns regions were mapped to their respective genes with the pc-HiC interaction maps. Overlap analysis was carried by GeneOverlap R package. P-value (numbers) and odds ratio (color) from Fisher's exact test are presented in the heatmap. n.s, not significant. **e**, Pearson correlation between log2FC values of DARs and log2FC of DEGs that were annotated to those region (intergenic regions were mapped via the pc-HiC data set). Chromatin accessibility changes were compared with parsed exonic reads (red line), intronic reads (blue lines) and total transcriptional changes (both intronic and exonic reads) as measured by Desq2 (gray line). All r and p-values are reported in Supplementary Table 9.

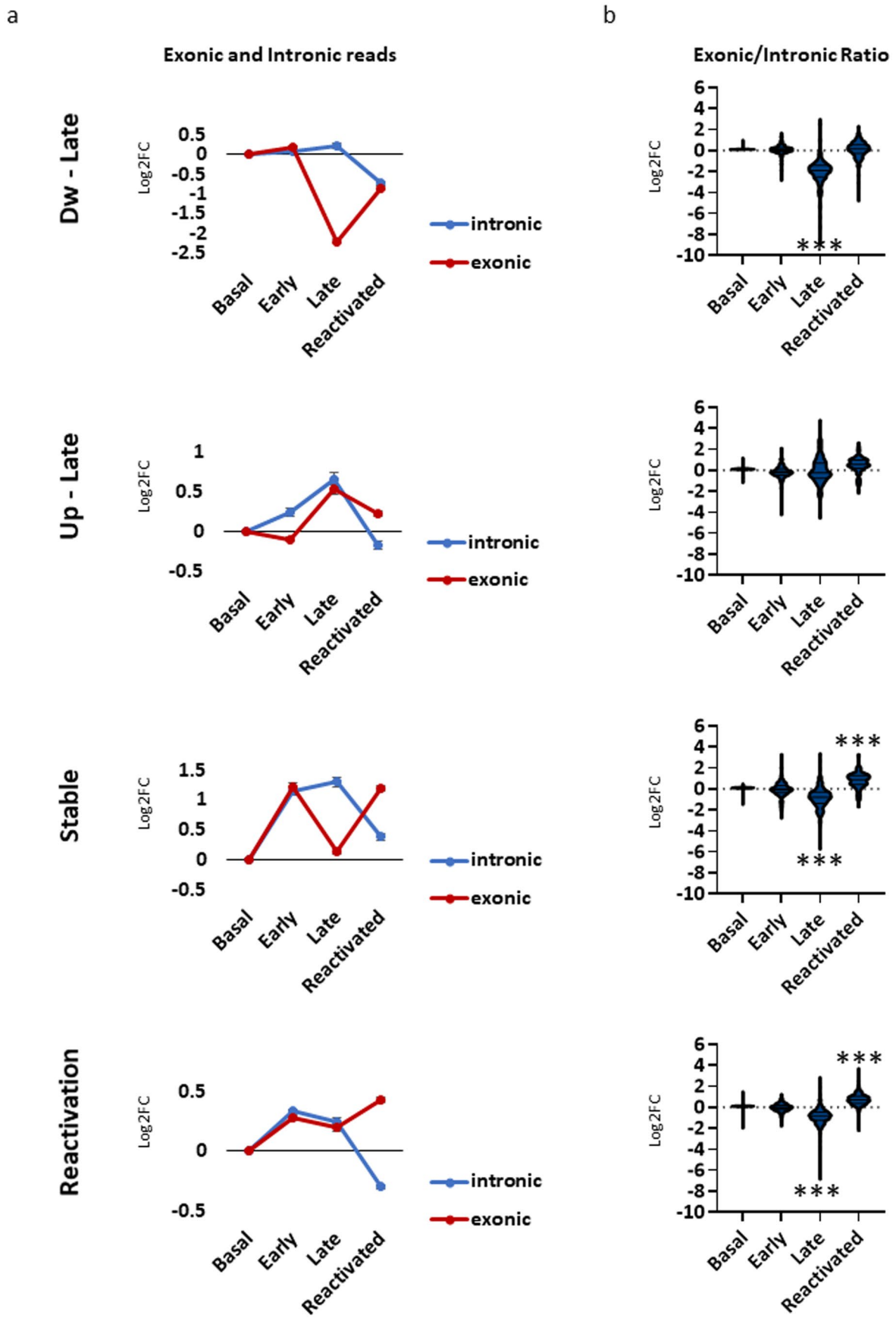

Extended Data Fig. 5 | See next page for caption.

Extended Data Fig. 5 | Transcriptional changes in the activated-late neurons correlated higher with intronic reads and reactivated neurons presented higher correlation with exonic reads. a, Exonic (red) and intronic (blue) reads were quantified separately across all conditions for each of the clusters identified in Fig. 5b. Reads were normalized (RPKM) and the log2FC changes are presented for each cluster. **b**, Exon/intron ratios were measured in each cluster across all conditions. Violin plot indicates the mean, interquartile range and the minimum and maximum, n = 3 biologically independent samples one-way ANOVA (parametric, unpaired), Dw–Late cluster; $F(3, 968) = 139.4$, $P < 0.0001$. Up -Late cluster; $F(3, 734) = 15.95$, $P < 0.0001$. Stable-cluster; $F(3, 652) = 93.97$, $P < 0.0001$. Reactivation cluster; $F(3, 1600) = 485.2$, $P < 0.0001$. Bonferroni's multiple comparisons test to Deseq2 reads. ***$P < 0.0001$.

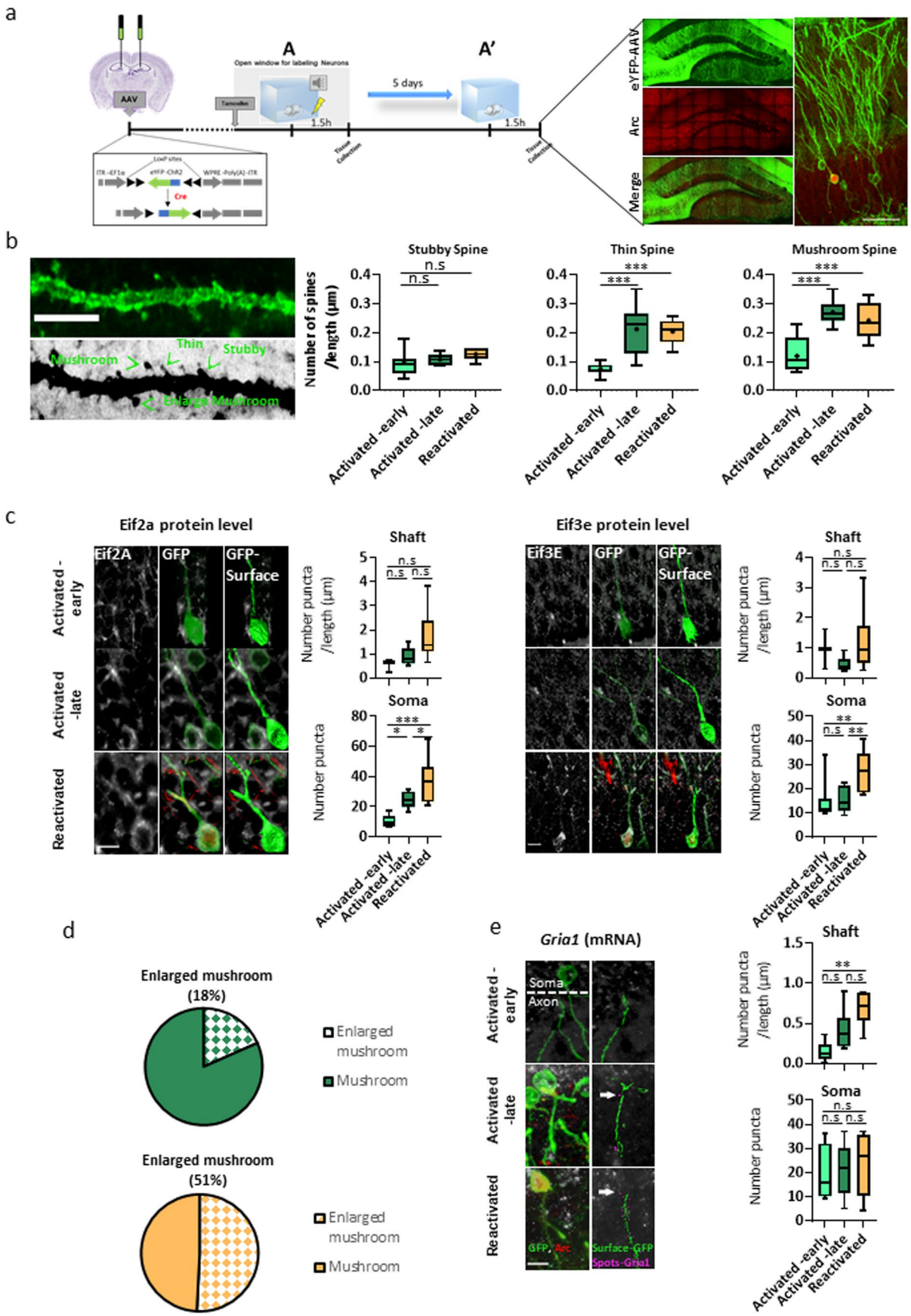

Extended Data Fig. 6 | See next page for caption.

Extended Data Fig. 6 | Distinct temporally transcriptional programs are being synchronized to maintain neuronal excitability, structural changes and protein translation in synapses in the engram ensemble. a, Schematics representation of the experimental design. Three weeks prior to the CFC test, ArcCreERT2 mice were bilaterally injected to the DG with AAV9-EF1a-DIO-hChR2-EYFP. In a similar manner to the TRAP system, eYFP reporter is only expressed in a Cre- dependent manner in the presence of tamoxifen. In the right panel, representative IHC images of the DG. Green—AAV-eYFP, Red—endogenous Arc. The scale bar represents 50 μm. **b**, Spines morphology assessment during different memory phases. Right panel shows a single eYFP+ dendritic shaft with different types of spines (Stubby, Thin, Mushroom, Enlarged mushroom). The scale bar represents 5 μm. boxplot indicates the mean, interquartile range and the minimum and maximum, Activated-early: n = 4 mice /5 section per animal, Activated-late: n = 4 mice /4 section per animal, Reactivated: n = 4 mice /2 section per animal. one-way ANOVA (parametric, unpaired), Stubby; $F(2, 36) = 2.313$, $P = 0.1135$. Thin; $F(2, 36) = 35.12$, $P < 0.0001$. Mushroom; $F(2, 36) = 38.42$, $P < 0.0001$. Bonferroni's multiple comparisons test, ***$P < 0.0001$. **c**, Representative IHC images and quantification of the protein levels of two members of the EIF family; (left) Eif2a and (right) Eif3e. The scale bar represents 10 μm. Data for dendritic shaft is presented as a ratio between number and the length (μM). n = 4 mice /5 section per animal, boxplot indicates the mean, interquartile range and the minimum and maximum, one-way ANOVA (parametric, unpaired) with Bonferroni's multiple comparisons test, n.s = not significant, Eif2a Shaft; $F(2, 20) = 4.484$, $P = 0.0246$. Soma; $F(2, 21) = 19.58$, $P < 0.0001$. (Activated-early vs. Activated-late *$P = 0.0142$, Activated-early vs. Reactivated *$P < 0.0001$, Activated-late vs. Reactivated *$P = 0.0303$). Eif3e Shaft; $F(2, 14) = 1.983$, $P = 0.1745$. Soma; $F(2, 23) = 8.309$, $P = 0.0019$, (Activated-early vs. Reactivated *$P = 0.0057$, Activated-late vs. Reactivated *$P = 0.0055$). **d**, Pie chart present the percentage of enlarged mushroom spines ($Dh \geq 3Dn$) and mushroom spines from Activated-late and Reactivated neurons. **e**, Representative images (left panel) and quantification (right panel) of Gria1 mRNA levels, during different phases of memory. Data is presented as a ratio between number of puncta and the dendritic shaft length. The scale bar represents 10 μm. N = 4 mice /5 section per animal, boxplot indicates the mean, interquartile range and the minimum and maximum, Shaft; one-way ANOVA (parametric, unpaired) $F(2, 15) = 10.41$, $P = 0.0015$. Bonferroni's multiple comparisons test, **$P = 0.0011$. lower panel - Soma; one-way ANOVA $F(2, 12) = 0.13$, $P = 0.88$.

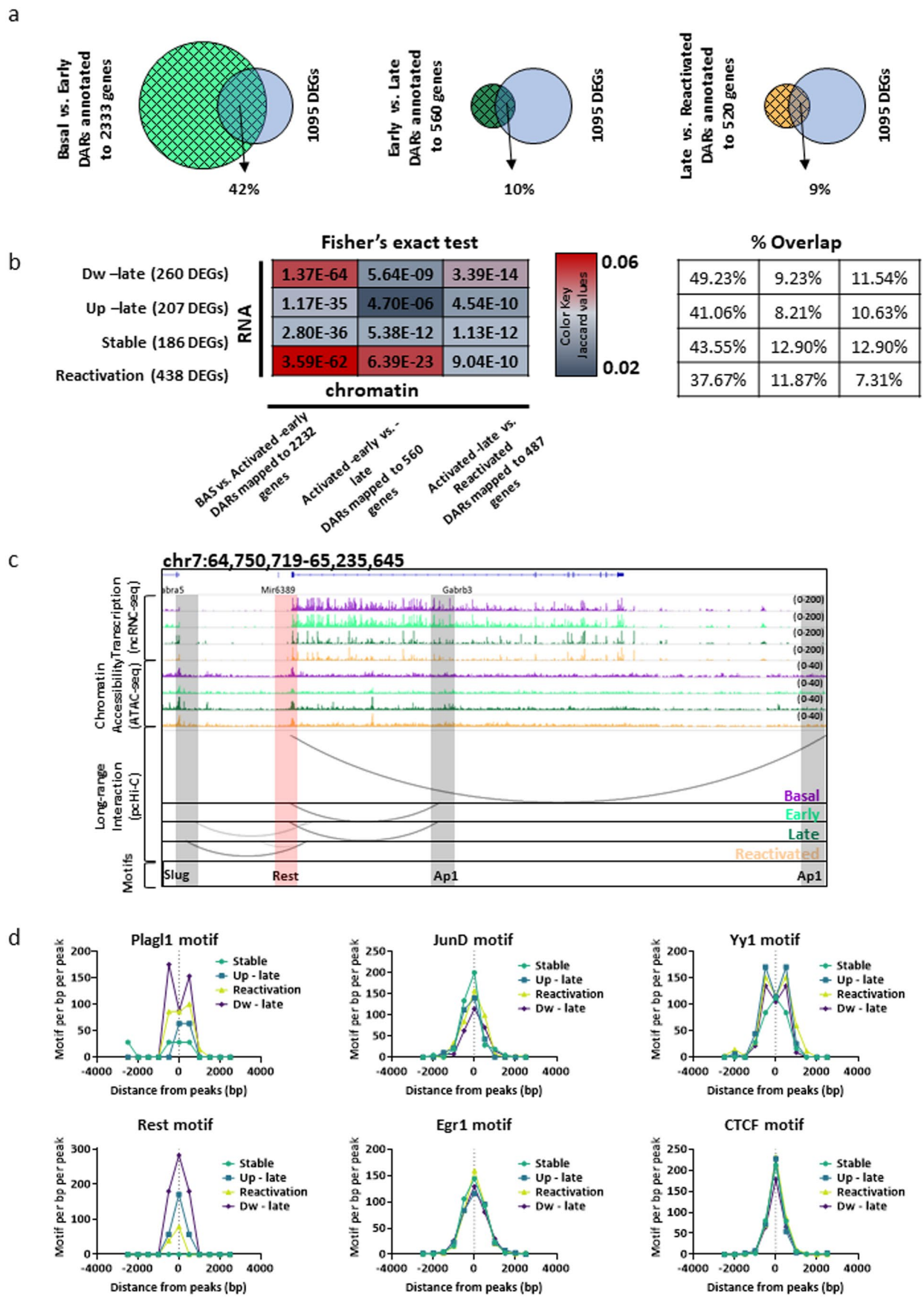

Extended Data Fig. 7 | See next page for caption.

Extended Data Fig. 7 | Interactions with distinct combinatorial enhancers leads to a directional change in gene expression. a, Venn diagrams shows percentage of overlap between chromatin accessibility (DARs) across all memory phases (BAS vs. Activated-early, light green grid circle; Activated -early vs. Activated-late, dark green grid circle; Activated-late vs. Reactivated, orange grid circle) and total transcriptional changes from all identified clusters (Dw–late, Up –late, Stable, Reactivation, blue grid circle). Intergenic and introns DARs were mapped to their respective genes with the pc-HiC interaction maps. Percentage of overlap was calculated from all identified DEGs in the clusters (n = 1095). **b**, Overlap analysis between DARs (pairwise) and DEGs from each cluster. Intergenic and introns DARs were mapped to their respective genes with the pc-HiC interaction maps. Overlap analysis was carried by GeneOverlap R package. P-values and Jaccard values (color) from Fisher's exact test are presented on the heat map (left). Percentage of overlap was calculated from all identified DEGs in the clusters (right). **c**, Representative image of chromatin and transcriptional changes of the Gabrb3 locus from the Dw-late cluster. While early state interactions were between promoter and enhancers with transcriptional activators (Ap1), late state interaction were with transcriptional repressors (Slug). Upper IGV genome browser tracks (purple - Basal, light green - Activated-early, dark green - Activated-late and orange - Reactivated) presenting transcriptional changes (nRNA-seq), middle tracks shows chromatin accessibility dynamics (ATAC-seq) on promoter (red rectangle) and enhancers (gray rectangle). Significant promoter-enhancer interaction are represented as arcs (WashU browser tracks). Lower track present motifs that were identified via HOMER tools (Slug, Ap1 and Rest). **d**, Aggregation plots for individual motifs. The enrichment values (motifs per bp/ per peak) of six selected motifs (two repressors, two activators and two bivalent) was assessed around the center of peaks (-/+ 4000 bp) from each cluster.

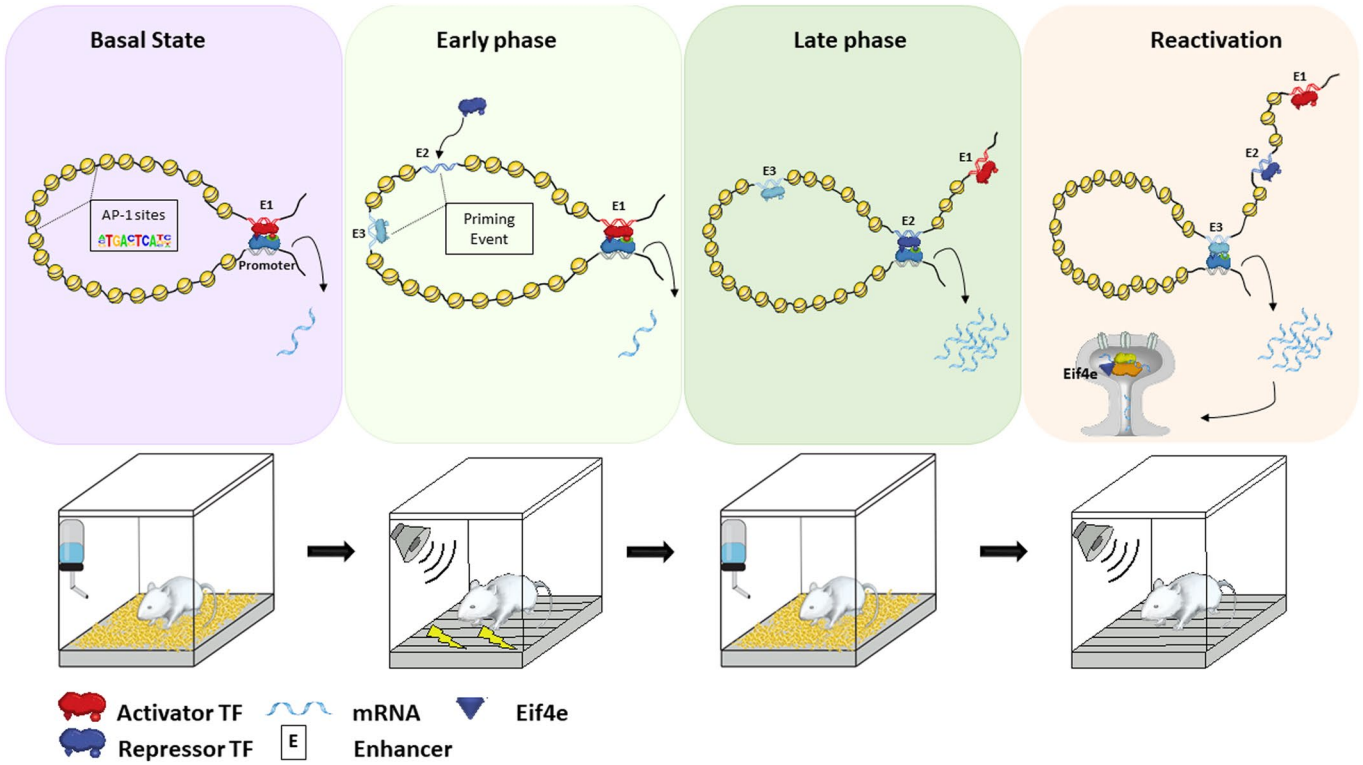

Extended Data Fig. 8 | Proposed model of the chromatin accessibility, promoter-enhancer interaction and transcriptional dynamics of hippocampal memory engram neurons. Over the course of memory formation and recall. Basal state - gene promoters interact with enhancers that carry transcriptional repressor cargo and express low levels of mRNA. Early phase - leads to a priming event, in which enhancers that harbor transcriptional activator cargo become more accessible, but most of them remain isolated and lack interactions with respective gene promoters. Late phase - gene promoters shift their interaction to the primed regions, which harbor transcriptional activator motifs. This promoter-enhancer reprograming results in increased gene expression that presumably allows the stabilization of the memory. Recall - reactivated engram neurons utilized a subset of primed promoter-enhancer interactions, which is associated with transcriptional changes involved in mRNA transport to synaptic compartments and protein translation. Transcription factor - TF, E(1–3)—different enhancer that interact with the same promoter, Red - transcriptional repressors, Blue - transcriptional activators.

nature research

Corresponding author(s): Asaf Marco, Li-Huei Tsai

Last updated by author(s): 6/25/2020

Reporting Summary

Nature Research wishes to improve the reproducibility of the work that we publish. This form provides structure for consistency and transparency in reporting. For further information on Nature Research policies, see our Editorial Policies and the Editorial Policy Checklist.

Statistics

For all statistical analyses, confirm that the following items are present in the figure legend, table legend, main text, or Methods section.

n/a	Confirmed
☐	☒ The exact sample size (*n*) for each experimental group/condition, given as a discrete number and unit of measurement
☐	☒ A statement on whether measurements were taken from distinct samples or whether the same sample was measured repeatedly
☐	☒ The statistical test(s) used AND whether they are one- or two-sided *Only common tests should be described solely by name; describe more complex techniques in the Methods section.*
☐	☒ A description of all covariates tested
☐	☒ A description of any assumptions or corrections, such as tests of normality and adjustment for multiple comparisons
☐	☒ A full description of the statistical parameters including central tendency (e.g. means) or other basic estimates (e.g. regression coefficient) AND variation (e.g. standard deviation) or associated estimates of uncertainty (e.g. confidence intervals)
☐	☒ For null hypothesis testing, the test statistic (e.g. *F*, *t*, *r*) with confidence intervals, effect sizes, degrees of freedom and *P* value noted *Give P values as exact values whenever suitable.*
☒	☐ For Bayesian analysis, information on the choice of priors and Markov chain Monte Carlo settings
☒	☐ For hierarchical and complex designs, identification of the appropriate level for tests and full reporting of outcomes
☐	☒ Estimates of effect sizes (e.g. Cohen's *d*, Pearson's *r*), indicating how they were calculated

Our web collection on statistics for biologists contains articles on many of the points above.

Software and code

Policy information about availability of computer code

Data collection	Nuclei were sorted with the flow cytometer FACS AriaIII (Becton Dickinson Biosciences, USA) Raw sequence data was generated by Illumina's Nextseq 550 (ATCA-seq, HiC, pc-HiC) and HiSeq 2000 platform (nRNA-seq). Real-time PCR data was generated by Bio-Rad CFX96 connect unit. Images were acquired using a LSM 710 or LSM 880 Zeiss confocal microscopes
Data analysis	Analysis ATAC-seq data: Sequence alignment: Bowtie2 (v2.3.0) BAM file processing: Samtools (v1.9macs2) Peak calling: MACS2 (v2.1.1) Differential peaks analysis: Diffbind (v2.10) Analysis Hi-C data: Sequence alignment and processing: HOMER (v4.1) and Juicer (v1.8.8) Analysis pcHi-C data: Sequence alignment: HiCUP (v0.6) BAM file processing and significant interaction analysis: CHiCAGO (v1.2.0) Analysis nRNA-seq data: Sequence alignment: Bowtie2 (v2.3.0) BAM file processing and differential analysis: Cufflinks (v2.2) and DESeq2 (v.1.22.2). Confocal images were analyzed with ImageJ (v1.51) and Imarisx64 BiTPlane software (v8.1.2). 3D images were converted from confocal image stacks. Proteins/mRNA levels were counted using the Surface-To-Surface and Close -To -Surface XTension modules.

FACS: Flowjo (v10).
Statistical analyses and visualization of data were performed using the GraphPad Prism (v8.2.1) and R-packages: ggplot2 (v3.1.0), circlize (v0.4.5), ComplexHeatmap (v1.2.0), gridExtra (v2.3), GeneOverlap (v1.18.0) and bedr (v1.0.6).
Other software for data analysis and visualization: Microsoft Excel, R Studio (v3.5.2), ChromHMM (v1.15), Bedtools (v2.25.0), DeepTools (v3.2.1), IGV (v2.3), Washu browser (v50.3.6).

For manuscripts utilizing custom algorithms or software that are central to the research but not yet described in published literature, software must be made available to editors and reviewers. We strongly encourage code deposition in a community repository (e.g. GitHub). See the Nature Research guidelines for submitting code & software for further information.

Data

Policy information about availability of data

All manuscripts must include a data availability statement. This statement should provide the following information, where applicable:

- Accession codes, unique identifiers, or web links for publicly available datasets
- A list of figures that have associated raw data
- A description of any restrictions on data availability

* GSE152956 is the reference Series:
https://www.ncbi.nlm.nih.gov/geo/query/acc.cgi?acc=GSE152956

* SubSeries that are linked to GSE152956:
https://www.ncbi.nlm.nih.gov/geo/query/acc.cgi?acc=GSE152775
https://www.ncbi.nlm.nih.gov/geo/query/acc.cgi?acc=GSE152953
https://www.ncbi.nlm.nih.gov/geo/query/acc.cgi?acc=GSE152954
https://www.ncbi.nlm.nih.gov/geo/query/acc.cgi?acc=GSE152955

Field-specific reporting

Please select the one below that is the best fit for your research. If you are not sure, read the appropriate sections before making your selection.

☒ Life sciences ☐ Behavioural & social sciences ☐ Ecological, evolutionary & environmental sciences

For a reference copy of the document with all sections, see nature.com/documents/nr-reporting-summary-flat.pdf

Life sciences study design

All studies must disclose on these points even when the disclosure is negative.

Sample size	In NGS experiments no statistical methods were used to pre-determine sample sizes. Sample sizes were chosen based on prior literature using similar experimental paradigms (Halder, R. et al. (2015), Fernandez-Albert, J. et al. (2019), Schoenfelder, S. et al. (2015)). Sample size was estimated according to data variance between biological replicates and distance to control condition (Basal group). In addition, sample size was determined to be adequate based on the magnitude and consistency of measurable differences between groups. Each analysis was done in accordance to the sample size, sequencing depth and conditions. Due to sample and animals limitation, no statistical methods were used to pre-determine sample sizes in 3C and ChIP-qPCR experiments. Sample sizes were chosen based on prior literature using similar experimental paradigms (Kagey MH et al. 2010. Mediator and cohesin connect gene expression and chromatin architecture. Nature 467: 430–435) In all other experiments, sample sizes were calculated by power analysis.
Data exclusions	1 (Basal) out of 13 ATAC-seq samples were excluded due to insufficient quality (less then 10,00 detected peaks), exclusion criteria was not pre-established. 1 (Early) out of 6 Hi-C samples were excluded due to insufficient quality (less then 10M reads and more then 40% of local interactions), exclusion criteria was not pre-established). In Figure 2a (Late vs. Reactivated) - one region from the chromatin differential analysis was discovered as an outlier and was excluded from the figure (xclusion criteria was not pre-established).
Replication	We used different cohorts and data types to replicate/validate our findings: 1. ATAC-seq: 3 biological replicates/ per group. 10,000 cells from each group, were pulled from 8-10 different mice and considered as N=1. Validation of chromatin accessibility with previous published ATAC-seq data (Su, Y. et al. (2016)) and ChIP-seq data (Halder, R. et al. (2015). 2. RNA-seq: 3 biological replicates/ per group. 10,000 cells from each group, were pulled from 8-10 different mice and considered as N=1. Validation of DEGs with previous published data in similar experiments conditions (Rao-Ruiz, P. et al. (2019), Jaeger, B. N. et al. (2018), Tyssowski, K. M. et al. (2018)). 3. pcHi-C: 3-4 biological replicates/ per group. 10,000 cells from each group, were pulled from 8-10 different mice and considered as N=1. Validation of promoter-enhancer interaction (number of significant long-range interactions per group, average of interacting enhancers per promoter) with previous published (Schoenfelder, S. et al. (2015)). 4. Hi-C: 2 biological replicates/ per group. 100,000 cells from each group, were pulled from 4-5 different mice and considered as N=1. In all experiments reproducibility across replicate was very high. The measures applied to evaluate replicates were correlation among samples, variance, principal component analysis (PCA) and statistical tests that revealed non significant differences within the group. ChromHMM analysis was validated by ChIP-qPCR experiments. pcHi-C was validated by independent 3C experiments. 5. In all NGS experiments, reproducibility across replicate was very high. The measures applied to evaluate replicates were correlation among samples, principal component analysis (PCA) and statistical tests that revealed non significant differences within the group. 6. All measurements were taken from distinct samples and the same sample was never measured repeatedly. 7. All IHC experiments were repeated independently with similar results.

Randomization	Set of mice with the same age were raised in the same conditions and randomly allocated to the different experimental groups.
Blinding	Blinding was not applied in the behavioral studies (CFC) and imaging acquisition because animals/samples need to be controlled by treatment or conditions. Individuals generating the NGS data were blinded to the outcome measures. Individuals preforming the imaging quantification analysis for Eif, Gria1 proteins/mRNA and Spines morphology were blinded to the groups.

Reporting for specific materials, systems and methods

We require information from authors about some types of materials, experimental systems and methods used in many studies. Here, indicate whether each material, system or method listed is relevant to your study. If you are not sure if a list item applies to your research, read the appropriate section before selecting a response.

Materials & experimental systems

n/a	Involved in the study
☐	☒ Antibodies
☒	☐ Eukaryotic cell lines
☒	☐ Palaeontology and archaeology
☐	☒ Animals and other organisms
☒	☐ Human research participants
☒	☐ Clinical data
☒	☐ Dual use research of concern

Methods

n/a	Involved in the study
☒	☐ ChIP-seq
☐	☒ Flow cytometry
☒	☐ MRI-based neuroimaging

Antibodies

Antibodies used

eIF3e polyclonal Rabbit (1:500, #PA529487, Thermo Fisher Scientific); Validated by vendor - https://www.thermofisher.com/antibody/product/eIF3e-Antibody-Polyclonal/PA5-29487

eIF2a monoclonal Mouse (1:500, #AHO0802, Thermo Fisher Scientific); Validation source: Mark D Trottier Jr et al. VSV replication in neurons is inhibited by type I IFN at multiple stages of infection. Virology. (2005)

eIF4E monoclonal (5D11) Mouse (1:500, #MA1-089, Thermo Fisher Scientific); Validation source: Jianjun Hu et al. Nuclear localization of EIF4G3 suggests a role for the XY body in translational regulation during spermatogenesis in mice. Biol Reprod (2018)

Arc polyclonal Rabbit (1:500,#156003, Synaptic Systems); Validation source: Larsen MH et al. Regulation of activity-regulated cytoskeleton protein (Arc) mRNA after acute and chronic electroconvulsive stimulation in the rat. Brain research, 10641-2: 161-5, (2005).

Arc monoclonal Mouse (1:200, #sc-17839, Santa Cruz Biotechnology); Validation source: Nair RR et al . Dynamic Arc SUMOylation and Selective Interaction With F-Actin-Binding Protein Drebrin A in LTP Consolidation In Vivo. Front Synaptic Neurosci (2017).

GFP polyclonal Goat (1:500, #NB100-1770, Novus Biologicals); Validation source: Neves J et al. MANF delivery improves retinal homeostasis and cell replacement therapies in ageing mice Exp. Gerontol. (2020).

GluR1 Polyclonal Rabbit (1:500, #MAB2263, Millipore); Validation source: Sephton CF et al. Activity-dependent FUS dysregulation disrupts synaptic homeostasis. Proceedings of the National Academy of Sciences of the United States of America, 111 E4769-78 (2014).

NeuN (Fox 3, Rbfox 3) polyclonal Guinea pig (1:1000, #266004, Synaptic Systems); Validation source: Morin LP et al. Neurons identified by NeuN/Fox-3 immunoreactivity have a novel distribution in the hamster and mouse suprachiasmatic nucleus. Brain research 1421: 44-51, (2011)

H3K4me1 Polyclonal Rabbit (5ug/ul, #ab8895, Abcam); Validation source: Martire S et al. Phosphorylation of histone H3.3 at serine 31 promotes p300 activity and enhancer acetylation. Nat Genet 51:941-946 (2019).

H3K27ac Polyclonal Rabbit (5ug/ul, #ab4729, Abcam); Validation source: Tambalo M et al. Enhancer activation by FGF signalling during otic induction. Dev Biol 457:69-82 (2020).

Validation

All the antibodies used in this study have been validated in mice for the application in which they were used.
IHC - validation data is available from the manufacturer website. GluR1, eIF3e, eIF2a and eIF4E antibodies were validated by adding secondary antibody controls (withdrawal of primary antibody).
FACS - we used appropriate negative and positive controls. Samples were tested on the FACS with i) no primary or secondary antibody (to determine autoflorescence) ii) only secondary antibody iii) only one primary antibody (NeuN, GFP, Arc).
ChIP-qPCR - All antibodies were ChIP Grade. Validation data for the Abcam anti-H3K4me1 is available at https://www.abcam.com/histone-h3-mono-methyl-k4-antibody-chip-grade-ab8895.html; for the Abcam anti-H3K27ac is available at https://www.abcam.com/histone-h3-acetyl-k27-antibody-chip-grade-ab4729.html

Animals and other organisms

Policy information about studies involving animals; ARRIVE guidelines recommended for reporting animal research

Laboratory animals	Experiments were conducted in male mice (mean 3-month old). Mouse strains were maintained in a pure C57BL/6J background. Strains are: Arc-cre/ERT2 (Denny CA et al., 2014; Jackson labs, stock #022357); R26R-STOP-floxed- yellow fluorescent protein(eYFP) (Srinivas S et al., 2001; Jackson labs, stock #006148)
Wild animals	The study does not involve the use of wild animals
Field-collected samples	The study does not involve field-collected samples
Ethics oversight	All mouse work was approved by the Committee for Animal Care (CAC) and the Division of Comparative Medicine at the Massachusetts Institute of Technology (MIT), Protocol #0618-044-21

Note that full information on the approval of the study protocol must also be provided in the manuscript.

Flow Cytometry

Plots

Confirm that:

☒ The axis labels state the marker and fluorochrome used (e.g. CD4-FITC).

☒ The axis scales are clearly visible. Include numbers along axes only for bottom left plot of group (a 'group' is an analysis of identical markers).

☒ All plots are contour plots with outliers or pseudocolor plots.

☒ A numerical value for number of cells or percentage (with statistics) is provided.

Methodology

Sample preparation	Mice were sacrified by decapitation, hippocampi were microdisected and immediately homogenized in ice cold PBS with protease inhibitors (Pi) (11836170001, Roche). For RNA-seq, Hi-C and capture-HiC experiments, the suspension was fixed with 1% (RNA, Hi-C) or 2% (pc-HiC) paraformaldehyde. After wash x2 (PBS), pellet was resuspended in 5 mL of hypotonic buffer (NF-1) and was dounce-homogenized. Suspension were collected all in a 15 mL conical tube, filtered with 70 µm mesh filter (08-771-2, Falcon) and incubated on ice for 30 min. Pelleted nuclei (all centrifuge were 4°C, 1,600 x g for 15 min) were resuspended in 10 mL PBS+1%BSA+Pi and incubated on ice for 1 h. Nuclei were spun down and the pellet was resuspended in 1 mL PBST+1%BSA+Pi and incubated with NeuN, Arc and GFP primary antibodies for overnight in 4°C. Unbound antibodies were washed out twice with 5 mL of PBST and finally resuspended in 1 mL PBS+1%BSA+Pi and secondary antibodies for 2-4 h at 4°C. Follow two washes, nuclei were resuspended in 0.5 mL (PBS+1%BSA+Pi) and filter with 40 µm mesh filter for FACS sorting. 4′,6-Diamidine-2′-phenylindole dihydrochloride (DAPI) was added directly to the FACS tubes (1:5000, 10236276001, Sigma-Aldrich).
Instrument	FACS Aria III (Becton Dickinson Biosciences, USA)
Software	Flowjo v10
Cell population abundance	Cell population abundance is detailed in Supplementary Table 1.
Gating strategy	Nuclei were gated first using forward and side scatter pulse area parameters (FSC-A and SSC-A) excluding debris, followed by exclusion of aggregates using pulse width (FSC-W and SSC-W). Next, nuclei samples were gated by their DAPI signal to exclude doublets and aggregates. Then isotype control staining was used to set NEUN+, ARC+ and GFP+ gates. In order to secure a homogeneous neuronal population, the NeuN+ population was gated before gating populations based on ARC+ and GFP+ and ARC+/GFP+ fluorescence. Before sorting experiments, we used appropriate negative and positive controls. Samples were tested on the FACS with i) no primary or secondary antibody (to determine auto-florescence levels) ii) only secondary antibody iii) only one primary antibody (NeuN, GFP, Arc).

☒ Tick this box to confirm that a figure exemplifying the gating strategy is provided in the Supplementary Information.